New insights into the role of *Cutibacterium acnes*-derived extracellular vesicles in inflammatory skin disorders

Maria Pol Cros[(1)] , Júlia Mir-Pedrol[(1)(2)], Lorena Toloza[(1)], Nastassia Knödlseder[(1)], Julien Maruotti[(3)], Marc Güell[(1)] and Maria-José Fábrega Fernández[(1)*].

[(1)] Department of Medicine and Life Sciences, Universitat Pompeu Fabra, Barcelona, ES [(2)]Universitaet Tuebingen Fachbibliothek Mathematik und Physik Tubingen, Baden-Württemberg, DE [(3)] Phenocell, Grasse, FR.

* maria-jose.fabrega@upf.edu

ABSTRACT

Background: *Cutibacterium acnes* is one of the most prevalent bacteria that form the human skin microbiota and, depending on multifactorial conditions, may act as an opportunistic skin pathogen or can help to maintain the skin homeostasis. Actually, different phylotypes of *C. acnes* have been associated with different degrees of acne vulgaris development, while others, such as the H1 subtype, have been detected in patients with non-acneic skin. However, due to the physiology of the skin, the skin microbiota neither has direct access to the skin's sebaceous glands nor to the main immune cells, as they are protected by a sebum layer. Therefore, the inter-kingdom communication relies on secreted factors and bacterial extracellular vesicles (EVs). In this context, the purpose of this project is to study the role of EVs secreted by three different phylotypes of *C. acnes* (A1 as pathogenic, H1 as beneficial and H2 as commensal).

Results: Main findings showed that the proteomic profile of the cargo embodied in the EVs reflects unique characteristics of the different *C. acnes* phylotypes in terms of lifestyle, survival and virulence. Moreover, *in vitro* skin models showed an extended pro-inflammatory modulation of A1 EVs, while H1 EVs displayed a high sebum-reducing potential.

Conclusions: This study has highlighted the role of *C. acnes* EVs as key modulators during skin alterations, specially H1 EVs as an alternative based-natural treatment to fight acne vulgaris symptomatology.

Keywords: Microbiome, Extracellular vesicles (EVs), *Cutibacterium acnes*, Skin inflammation and Acne vulgaris.

1. INTRODUCTION

The human body harbours a flourishing diversity of microbes that form a dynamic and functional system that develops in synergy with the physiological development of its host (Rackaityte & Lynch, 2020). The human microbiome resides primarily in the skin, the oral mucosa and the gastrointestinal tracts (Paetzold et al., 2019). Recent data demonstrates that the specific composition of the microbial community is associated with health and disease, which suggests that a detailed characterization of the microbial community would reveal important commensal host-microbiome as well as microbe-microbe interactions with therapeutic implications (Blum, 2017). Over the past decade, researchers have discovered evidence of extensive communication between bacteria, skin cells and immune cells. These interactions are aimed at strengthening and repairing the barrier formed by the skin, reinforcing the body's defences against infection and reducing excess inflammation (Eisenstein, 2020). Nonetheless, failure of this communication can disrupt the protective barrier of the skin and lead to dysbiosis between commensals and pathogens.

One of the most common bacteria present in the normal human skin microbiota is the Gram-positive anaerobic bacterium, *Cutibacterium acnes* (*C. acnes*) which dominates the pilosebaceous units (McLaughlin et al., 2019). *C. acnes* helps to preserve and support the natural microbial balance of the skin but under certain conditions, it can also substantially alter its local environment and cause disease (Christensen et al., 2016; O'Neill & Gallo, 2018; Shu et al., 2013). In fact, this bacterium is linked to a wide range of skin diseases, including acne vulgaris. Although the aetiology and pathogenesis of acne are still uncertain, microbiome alterations are thought to be

52 one of the principal mechanisms behind the development of acne (Paetzold et al., 2019). Recently,
53 some authors have described that different phylotypes of *C. acnes* have different degrees of
54 association with acne vulgaris (Fitz-Gibbon et al., 2013; Lomholt & Kilian, 2010; McDowell et
55 al., 2013; McLaughlin et al., 2019). This brings into question how bacteria communicate with
56 host cells to maintain homeostasis of the skin microbiota if sebaceous glands and immune cells
57 are protected by a layer of sebum from external environment and skin microorganisms. This
58 communication is known to be mediated by bacterial extracellular vesicles (EVs), which are nano-
59 sized lipid bilayer vesicles approximately 20-500 nm in diameter that can pass through the lipid
60 barrier and interact with host cells (Bajic et al., 2020; Brown et al., 2015).
61 Since EVs play a key role in interkingdom communication and immune modulation, in the present
62 study, different *in vitro* models mimicking human skin have been established to assay the
63 potential of different *C. acnes* EVs. In this context and based on previous publications (Choi et
64 al., 2018a; Chudzik et al., 2022; Paetzold et al., 2019), we decided to study the role that EVs from
65 three different phylotypes of *C. acnes* play in the onset of acne, considering *C. acnes* A1
66 phylotype (clade IA1) as a pathogenic phylotype, *C. acnes* H1 phylotype (clade IB) as a probiotic
67 phylotype, and *C. acnes* H2 phylotype (clade IB) as a commensal one. Moreover, proteomic
68 characterization of *C. acnes* A1, H1 and H2 EVs has been carried out to determine the relationship
69 of their protein cargo with the skin microbiota. Finally, a novel model mimicking acne-prone skin
70 has been set up in which the sebum-reducing potential of EVs from different *C. acnes* phylotypes
71 has also been tested.
72

73 ## 2. MATERIALS AND METHODS

74 ### 2.1 Bacterial phylotypes and culture conditions

75 *C. acnes* phylotypes used in this study were extracted from healthy human skin (A1 and H1) or
76 commercially acquired (H2, KPA17202 from DSMZ), typed by SLST typing and we previously
77 sequenced. Sequencing data can be found in the European nucleotide Archive under project
78 number PRJEB42527.

79 Initial cultures were always started from glycerol stocks (stored at −80°C) and seeded on Brucella
80 agar plates which were incubated for 4-5 days at 37°C under anaerobic conditions using the BD
81 GasPak EZ anaerobic bag system.

82 **2.2 Isolation of EVs**

83 The process followed for the isolation of EVs consisted of several steps: cultivation,
84 centrifugation, concentration or ultrafiltration and ultracentrifugation (Fig. S1).

85 In the cultivation step, *C. acnes* phylotypes A1, H1 and H2 were collected from a Brucella agar
86 plate using sterile swabs (Deltalab) and were transferred into 1 L of Brucella liquid medium. After
87 7 to 10 days at 37°C with 300 rpm of stirring and maintaining anaerobic conditions, the culture
88 was centrifuged in 250 mL sterile bottles at 10,000 x g for 30 min and at 4°C. For this step, a
89 Beckman Coulter Avanti JXN-26 high-velocity centrifuge with the J-LITE JLA-16.250 Fixed-
90 Angle Aluminium Rotor were used. Then, the pellet was discarded, and the supernatant (SN) was
91 filtered using the Thermo Scientific Nalgene Rapid-Flow 75 mm Filter Unit (500 mL) to avoid
92 bacterial contamination. Afterwards, the SN was concentrated by a Centricon Plus-70 10 KDa
93 system using the JS-5.3 Swinging-Bucket Rotor. To ensure free contamination during the process,
94 an extra step of 0.22 μm filtration was added to the protocol. The filtered and concentrated SN
95 was then ultra-centrifuged in a Beckman Coulter optima L-100 XP ultracentrifuge using the
96 SW41 Ti Swinging-Bucket Rotor at 154,300 x g for 2h and at 4°C to precipitate the EVs. The
97 pellet containing the isolated *C. acnes* EVs was washed with 1X phosphate buffered-saline (PBS)
98 buffer and ultra-centrifuged again for 1h under the same conditions as in the previous step.
99 Finally, the SN was discarded, and the pellet was resuspended with 200 μL of PBS buffer and
100 kept in an Eppendorf at −20°C. To ensure non-bacterial presence in EVs samples, 10 μL of each
101 batch were seeded in a Brucella agar plate and incubated for 4-5 days at 37°C under anaerobic
102 conditions.

103 **2.3 EVs labelling protocol**

104 EVs labelling was performed as previously described by (Bajic et al., 2020; Cañas et al., 2016;
105 Fábrega et al., 2017). Briefly, isolated A1 EVs were resuspended in PBS buffer, centrifuged at
106 154,300 x g for 2h at 4°C, and resuspended in labelling buffer (50 mM Na_2CO_3, 100 mM NaCl,
107 pH 9.2) in the presence of 1 mg/mL of octadecyl rhodamine B-R18 (Invitrogen) and incubated
108 for 1 h at 25°C. Labelled A1 EVs were pelleted by ultracentrifugation at 154,300 x g for 1h at
109 4°C, resuspended in PBS buffer (0.2 M NaCl) and washed three times to fully remove the
110 unbound dye. After the final ultracentrifugation step, B-R18 labelled A1 EVs were resuspended
111 in PBS buffer (0.2 M NaCl) containing a protease inhibitory cocktail (Complete Protease
112 Inhibitory Tablets, Roche) and were stored at -20°C.

113 **2.4 Negative staining and Transmission Electron Microscopy (TEM)**

114 Isolated *C. acnes* H1 EVs were examined by TEM after negative staining, as described in previous
115 publications (Aguilera et al., 2014). In this particular case, EVs were resuspended in TRIS buffer
116 as PBS buffer is not compatible with uranyl acetate. A drop of EVs suspension was absorbed for
117 2 min on Formvar/carbon-coated grids that were previously activated with UV light. The grids
118 were washed with distilled water, stained with 2% uranyl acetate for 1 min, air dried and examined
119 by TEM (*Parc Científic de Barcelona*).

120 **2.5 Nanoparticle Tracking Analysis (NTA) of EVs**

121 EVs resuspended in 200 µL of PBS buffer were sent to *Institut de Ciència de materials de*
122 *Barcelona* to be examined with the Malvern Nanosight NS300 instrument. This system uses NTA
123 technology characterize nanoparticles in suspension in the size range of 10-2000 nm. A video is
124 taken and the NTA software tracks the Brownian motion of individual EVs and calculates their
125 size and total concentration.

126 **2.6 Determination of protein concentration and SDS-PAGE**

127 Protein concentrations in EVs samples were determined using the Qubit Protein Assay Kit
128 (Thermo Fisher Scientific). Measuring was done using the Qubit Fluorometer (Thermo Fisher
129 Scientific). This assay was performed at room temperature using specific Qubit assay tubes (Cat.
130 no. Q32856).

131 For protein separation, the samples were subjected to sodium dodecyl sulfate-polyacrylamide gel
132 electrophoresis (SDS-PAGE) using the Mini Gel Tank electrophoresis system (Invitrogen).
133 Proteins were denatured in a loading buffer (4X LDS sample buffer + β -mercaptoethanol) at
134 98°C for 5 min. Then, 10 µL of PageRuler Protein Ladder and 7 µg of each sample of proteins
135 mixed with 5 µL of loading buffer were loaded and separated on a NuPAGE 4 to 12% Bis-Tris
136 Gel (Invitrogen) using MOPS SDS Running Buffer 20X (Life technologies) at a constant voltage
137 of 100 V and for 40 min. After the run was completed, several bands were identified. Gel images
138 were visualized in the ChemiDoc MP Imaging System (Bio-Rad).

139 **2.7 Proteomic analysis: EVs preparation**

140 EVs were lysed to get a total representation of their protein content. To do that, liquid nitrogen
141 (N_2) was used to obtain beads of the EVs solutions of each *C. acnes* phylotype. Then, 0.5 g of
142 beads were disrupted using the Freezer Mill. Conditions used for the lysis were: precooling for 5
143 min, running step for 2 min, 2 cycles of interval and at a rate of 10 cycles per second (CPS). The
144 powder obtained was resuspended in RIPA buffer supplemented with complete protease
145 inhibitory tablets (Roche). Afterwards, total protein was precipitated with acetone and the final
146 precipitate was resuspended with a quantity ranging from 50 µL to 250 µL of 6 M urea to have a
147 minimum of 8 µg of protein. Qubit protein assay was performed to determine the estimated
148 quantity of protein in each EV sample.

149 **2.8 Identification of EVs proteins by LC-MS/MS analysis**

150 For the identification of the EVs proteins, mass spectrometry was performed by the UPF/CRG
151 Proteomics Unit.

152 Samples (8 µg) were reduced with dithiothreitol (24 nmol, 37°C, 60 min) and alkylated in the
153 dark with iodoacetamide (48 nmol, 25°C, 30 min). The resulting protein extract was first diluted
154 to 2M urea with 200 mM ammonium bicarbonate for digestion with endoproteinase Lys-C (1:10
155 w:w, 37°C, o/n, Wako, cat # 129-02541), and then diluted 2-fold with 200 mM ammonium
156 bicarbonate for trypsin digestion (1:10 w:w, 37°C, 8h, Promega cat # V5113). After digestion,
157 the peptide mix was acidified with formic acid and desalted with a MicroSpin C18 column (The
158 Nest Group, Inc) prior to LC-MS/MS analysis.

159 Afterwards, samples were analysed using the LTQ - Orbitrap Fusion Lumos mass spectrometer
160 (Thermo Fisher Scientific, San Jose, CA, USA) coupled with an EASY-nLC 1200 (Thermo Fisher
161 Scientific (Proxeon), Odense, Denmark). Peptides were loaded directly onto the analytical
162 column and were separated by reversed-phase chromatography using a 50-cm column with an
163 inner diameter of 75 µm, packed with a 2 µm C18 particles spectrometer (Thermo Scientific).

164 Chromatographic gradients started at 95% buffer A and 5% buffer B with a flow rate of 300
165 nL/min for 5 min and gradually increased to 25% buffer B and 75% A in 79 min and then to 40%
166 buffer B and 60% A in 11 min. After each analysis, the column was washed for 10 min with 10%
167 buffer A and 90% buffer B. Buffer A: 0.1% formic acid in water. Buffer B: 0.1% formic acid in
168 80% acetonitrile.

169 The mass spectrometer was operated in positive ionization mode with nanospray voltage set at
170 2.4 kV and source temperature at 305°C. The acquisition was performed in data-dependent
171 acquisition (DDA) mode and full MS scans with 1 micro scan at a resolution of 120,000 were
172 used over a mass range of m/z 350-1400 with detection in the Orbitrap mass analyser, auto gain
173 control (AGC) was set to "Standard" and maximum injection time to "Auto". In each cycle of
174 data-dependent acquisition analysis, following each survey scan, the most intense ions above a
175 threshold ion count of 10000 were selected for fragmentation. The number of selected precursor
176 ions for fragmentation was determined by the "Top Speed" acquisition algorithm and a dynamic
177 exclusion of 60 seconds. Fragment ion spectra were produced via high-energy collision

178 dissociation (HCD) at a normalized collision energy of 28% and they were acquired in the ion
179 trap mass analyser. AGC was set to 2E4, and an isolation window of 0.7 m/z and a maximum
180 injection time of 12 ms were used. Digested bovine serum albumin (New England Biolabs cat #
181 P8108S) was analysed between each sample to avoid sample carryover and to assure stability of
182 the instrument and QCloud (Chiva et al., 2018) has been used to control instrument longitudinal
183 performance during the project.

184 Acquired spectra were analysed using the Proteome Discoverer software suite (v2.0, Thermo
185 Fisher Scientific) and the Mascot search engine (v2.6, Matrix Science (Perkins et al., n.d.)). The
186 data were searched against NCBI *Cutibacterium acnes* phylotype H2171202 database (as in
187 August 2021, 2476 entries, https://www.ncbi.nlm.nih.gov/nuccore/NC_006085.1). For peptide
188 identification a precursor ion mass tolerance of 7 ppm was used for MS1 level, trypsin was chosen
189 as the enzyme, and up to three missed cleavages were allowed. The fragment ion mass tolerance
190 was set to 0.5 Da for MS2 spectra. Oxidation of methionine and N-terminal protein acetylation
191 were used as variable modifications whereas carbamidomethylation on cysteines was set as a
192 fixed modification. The false discovery rate (FDR) in peptide identification was set to a maximum
193 of 5%. Peptide quantification data were retrieved from the "Precursor ion area detector" node
194 from Proteome Discoverer (v2.0) using 2 ppm mass tolerance for the peptide extracted ion current
195 (XIC). The obtained values were used to calculate protein fold-changes and their corresponding
196 adjusted p-values.

197 **2.9 Bioinformatic analysis**

198 Proteins found by mass spectrometry were annotated from the UniProt database (UniProt
199 Consortium, 2021). Pseudo proteins or proteins lacking information in UniProt were removed
200 from the analysis. Only proteins with an area found in two or three of the replicas were considered.
201 The mean of the areas of each protein was calculated.
202

203 Proteins present only in one of the three phylotype EVs were selected for further analysis. The
204 information on biological processes, cellular components and molecular functions was obtained
205 and manually curated to classify each protein into a category.

206 **2.10 *In vitro* human cell lines maintenance**

207 The immortalized keratinocytes cell line (HaCaT), bought in the American Type Culture
208 Collection (ATCC), were cultured in T-75 culture flasks (Thermo Scientific) with Dulbecco's
209 Modified Eagle Medium (DMEM, Gibco) supplemented with 10% of Fetal Bovine Serum (FBS)
210 and 0.1% of penicillin and streptomycin. They were incubated at 37°C in 5% of CO_2, and 95% of
211 humidity until 90-100% of confluency.

212 The immortalized sebocytes cell line (SZ95) was donated by the Laboratory for Biogerontology,
213 Dermato-Pharmacology and Dermato-Endocrinology at the Departments of Dermatology,
214 Venereology, Allergology and Immunology of the Dessau Medical Centre. Sebocytes were
215 cultured in T-75 culture flasks (Thermo Scientific) with Sebomed basal medium (DMEM/F12,
216 Gibco) supplemented with 10% of FBS, 0.1% of penicillin and streptomycin, 5 ng/mL of
217 recombinant human epidermal growth factor (EGFr) and 500 µL of filtrated calcium chloride
218 ($CaCl_2$) 1M. They were incubated at 37°C in 5% of CO_2, and 95% of humidity until 90-100% of
219 confluency.

220 The immortalized T lymphocytes cell line (Jurkat, Clone E6-1), bought in the ATCC, were
221 cultured in T-75 culture flasks (Thermo Scientific) with Roswell Park Memorial Institute medium
222 (RPMI, Gibco) supplemented with 10% of FBS and 0.1% of penicillin and streptomycin. They
223 were incubated at 37°C in 5% of CO_2, and 95% of humidity until 90-100% of confluency.

224 PCi-SEB, derived from human iPSC with a Caucasian phototype (Phenocell), were seeded at a
225 density of 25.000 viable cells/cm^2 on fibronectin-coated tissue culture plate (Falcon) in
226 PhenoCULT-SEB basal medium supplemented with 0.1% of supplement A. Then, the media was
227 changed and supplemented with 0.1% of supplement M and incubated for 2 days more until cells

228 reached 90% of confluence and they were differentiated into mature sebocytes. Cells were
229 incubated at 37°C in 5% CO_2 and 95% of humidity during the whole differentiation process.

230 **2.11 Internalization of labelled-EVs**

231 To monitor EVs uptake by both HaCaT and SZ95, a total of $1 \cdot 10^5$ cells were seeded in an 8-well
232 chamber slider (Ibidi) until approximately 80% of confluence. Before the assay, the medium was
233 aspirated and replaced with rhodamine B-R18-labelled A1 EVs (2 µg/mL) suspended in DMEM
234 and Sebomed both without fetal bovine serum and red phenol. The cells with the labelled A1 EVs
235 were incubated at 37°C in 5% of CO_2, and 95% of humidity for 24h.

236 **2.12 Confocal fluorescence microscopy**

237 Cells were fixed for 30 min with 3% of paraformaldehyde at room temperature (RT) and washed
238 with PBS buffer to eliminate possible EVs residues. Plasma membranes were labelled with
239 fluorescent Alexa-488 wheat germ agglutinin (WGA) (Invitrogen) and nuclei with Hoechst
240 (Invitrogen). For this, cells were incubated for 25 min with Alexa-488 WGA (1 µg/mL) and
241 during 10-15 min with Hoechst (3 drops/mL). After PBS buffer washing, Ibidi mounting medium
242 was added (3 drops/well) to prepare the cells for microscopic visualisation.
243
244 Confocal microscopy was carried out using a ZEISS LSM 980 with Airyscan 2 confocal
245 microscope, using the 63x oil immersion objective lens. Fluorescence was recorded at 405 nm
246 (blue; Hoechst), 488 nm (green; WGA) and 546 nm (red; rhodamine B-R18). Z-stack images
247 were taken at 1.0-µm. Images were analysed using the Fiji image processing package.

248 **2.13 Cytotoxicity assay**

249 To evaluate cytotoxicity, an XTT Cell Viability Assay (Invitrogen) was performed following the
250 manufacturer's protocol. The assay kit includes the XTT reagent and an Electron Coupling

251 Reagent. In this case, the XTT reagent, is sensitive to cellular redox potential and in the presence
252 of live cells converts from a water-soluble compound to an orange-coloured formazan product.
253 $2 \cdot 10^5$ cells/mL of HaCaT and SZ95 were seeded in two different 96-well plates. After 24h, cells
254 were incubated with 1.56 µg/mL, 3.125 µg/mL, 6.25 µg/mL, 12.5 µg/mL, 25 µg/mL, 50 µg/mL,
255 100 µg/mL and 200 µg/mL of *C. acnes* A1, H1 and H2 EVs for 24h at 37°C in 5% of CO_2 and
256 95% of humidity. Then, 70 µL of working solution (XTT reagent) were added directly to each
257 well. Cells were incubated for 4h at 37°C in 5% of CO_2 and 95% of humidity. After incubation,
258 the absorbance was measured in the plate reader (Tecan) at 450 nm and 660 nm to eliminate the
259 background signal contributed by cell debris or other non-specific absorbance. Negative controls
260 with non-treated cells were included as blanks.
261 The percentage of cell viability was calculated using the following formula:

262 $$\% \text{ Cell Viability} = \frac{\text{Absorbance in Test well}}{\text{Absorbance in Blank well}} \cdot 100$$

263 **2.14 *C. acnes* EVs incubation in the outer skin layer model, the sebum model and the broken**
264 **skin barrier model**

265 *C. acnes* A1, H1 and H2 EVs were incubated with the immortalized HaCaT, SZ95 and Jurkat cell
266 lines (Fig. S2). For this purpose, $2 \cdot 10^5$ cells/mL were seeded in a 12-well plate for the three cell
267 lines. After 24h, all cell types were incubated for 24h with *C. acnes* A1, H1 and H2 EVs. The
268 three plates were divided into three rows - one for each *C. acnes* phylotype - and each row had a
269 control well and different concentrations of EVs, namely 12.5 µg/mL, 25 µg/mL and 50 µg/mL.

270 **2.15 Quantitative Real Time-PCR analysis (RT-qPCR)**

271 Total RNA was extracted from HaCaT, sebocytes and Jurkat cells using the miRNeasy Mini Kit
272 (Qiagen) following the manufacturer's recommendations. Purity and RNA concentration were
273 measured by the absorbance ratio at 260 and 280 nm on the NanoDrop One spectrophotometer
274 (Thermo Scientific).

275 RNA was reverse transcribed using the cDNA Reverse Transcription Kit (Thermo Fisher
276 Scientific) in a final volume of 20 µL following the manufacturer's protocol. The retro
277 transcription reaction was performed in the ProFlex PCR System (Applied Biosystems). RT-
278 qPCR reactions were performed on the QuantStudio 7 Flex Real-Time PCR System (Applied
279 Biosystems) using SYBR Green PCR Master Mix (Applied Biosystems) and cell-type specific
280 primers. See the list of primers in Table S4 of the Supporting Information. A control reaction was
281 set up with water in which no RNA was present. The $2^{-\Delta\Delta Ct}$ method was used to normalise
282 expression results. The values of the housekeeping CREBBP gene were used to standardise the
283 values obtained for each of the genes being studied.

284 **2.16 Multiplex panel (Eve Technologies)**

285 To validate the results obtained in the RT-qPCR, a Human High Sensitivity Plex Discovery Assay
286 was performed (Eve Technologies). The targets of interest were selected from an extensive list of
287 analytes and the company allowed multiplexing the previously selected targets together in a single
288 assay. Among all the analytes, the ones that stood out for us in the present project were cytokines
289 and chemokines.

290 **2.17 Evaluation of sebum-reducing potential of *C. acnes* A1, H1 and H2 EVs in the acne-**
291 **mimicking skin model**

292 For the acneic model, human iPSC-derived sebocytes (PCi-SEB) were incubated for 5 days with
293 maturation supplement. After that, the sebum production was induced by 48h of treatment with 5
294 µM of arachidonic acid (AA5). Then, cells were treated with 12.5 µg/mL of *C. acnes* A1, H1 and
295 H2 EVs for 24h and cells were fixed until sebum production determination. In parallel, non-
296 treated cells were used as negative control. For lipid droplets detection, cells were stained with
297 the fluorescent marker BODIPY 493/503 (Sigma Aldrich) following manufacture's
298 recommendations. The nucleus was stained with DAPI. Samples were analysed by confocal
299 fluorescence microscopy.

300 **2.18 Statistical analyses**

301 Statistical analyses were performed with GraphPad software. All tests were repeated
302 independently at least three times in triplicate. The values for all measurements are presented as
303 the mean ± standard deviation (SD). Differences between more than two groups were assessed
304 using one-way or two-way ANOVA followed by Dunnett's test. Data with a p-value less than
305 0.05 and less than 0.001 were considered statistically significant and statistically highly
306 significant, respectively.

307 **3. RESULTS**

308 **3.1 Isolation and visualization of *C. acnes* EVs**

309 *C. acnes* H1 EVs were isolated from cell-free culture supernatants (Fig. 1) and evaluated by
310 negative stain-TEM. Images displayed spherical vesicles approximately 70-100 nm in diameter
311 (Fig. 2A). To validate the TEM results and to obtain additional information, NTA which is a more
312 precise imaging technique, was carried out in *C. acnes* A1, H1 and H2 EVs. This last analysis
313 provided high-resolution particle size distribution profiles and also concentration measurements.
314 Fig. 2B shows the size distribution graphs of the different *C. acnes* EVs. On the other side, values
315 obtained after NTA revealed that H2 EVs have the largest mean vesicle size. However, in terms
316 of concentration, A1 is the phylotype with the highest EV secretion yield rate ($3.92 \cdot 10^{12}$
317 EVs/mL). Moreover, recordings of the different types of *C. acnes* EVs were acquired from the
318 NTA analysis (see Videos).

319 **3.2 Proteomic analysis comparison between *C. acnes* A1, H1 and H2 EVs**

320 SDS-PAGE analysis showed that EV triplicates of each phylotype display similar protein profiles
321 with slight differences (Fig. 3A), which is consistent with the suggested variability of protein
322 cargo between batches (Gandham et al., 2020; Hartjes et al., 2019a, 2019b; Paganini et al., 2019).
323 Furthermore, it should be noted that, although the same amount of protein was loaded into the gel
324 for the EVs of each phylotype (7 µg), the diversity of proteins is much higher in A1 EVs (clade

325 IA1) than in H1 and H2 EVs (clade IB). These findings are in line with the ones obtained by
326 Chudzik et al.
327 To characterize the protein profile of *C. acnes* A1, H1 and H2 EVs, the protein content was
328 isolated and examined by mass spectrometry by the UPF/CRG Proteomics Facility. As Fig. 3B
329 illustrates in a Venn diagram, the three phylotypes share 382 proteins. Additionally, a pairwise
330 comparison was performed, and the results showed that A1 and H1 share 171 proteins, A1 and
331 H2 share 66 proteins and H1 and H2 share 72 proteins.
332 Finally, observing the proteins exclusive to each phylotype it is shown that A1 EVs have the
333 highest number of high-confidence proteins identified, namely 396, followed by H1 and H2 EVs.
334 Using the UniProt database, a Gene Ontology (GO) and bioinformatics analysis were conducted
335 (Fig. 3C). In terms of biological processes, *C. acnes* A1 EVs were significantly enriched in
336 proteins participating in biosynthetic processes (22.77%) and metabolic processes (20.98%).
337 Regarding the molecular functions, binding (19.64%), transferase activity (14.29%) and
338 hydrolase activity (8.48%) were the most prevalent. For biological processes, proteins linked to
339 *C. acnes* H1 EVs were significantly enriched in transport (27.69%) and metabolic processes
340 (13.85%). Regarding the molecular functions, transporter activity (21.54%) and binding (16.92%)
341 were noteworthy. The predominant proteins involved in the biological processes of *C. acnes* H2
342 EVs were linked to transport (18.18%) and response to stimulus (9.09%). Regarding the
343 molecular functions of the vesicular proteins found in this phylotype, transporter activity
344 (27.27%), and oxidoreductase activity (18.18%) were the most prevalent. For all three types of
345 EVs, in terms of cellular components, the highest percentage of proteins were membrane-
346 associated proteins, followed by cytoplasmic proteins. Also, approximately 6-18% of the total
347 number of proteins were not properly classified as they were unknown or poorly characterized.
348 The identified proteins in *C. acnes* A1, H1 and H1 EVs are listed respectively in Tables S1, S2
349 and S3 of the Supporting Information.

350 **3.3 EVs from *C. acnes* A1 phylotype are internalized into keratinocytes and sebocytes**

351 *C. acnes* EVs internalization in HaCaT (keratinocytes) and SZ95 (sebocytes) cell lines was
352 confirmed by confocal fluorescence microscopy at 24h of incubation with rhodamine B-R18-
353 labeled A1 EVs (2 µg/ well). Membranes were labelled with WGA and nuclei with Hoechst. As
354 anticipated, no red signal was observed in untreated control cells (Fig. 4).

355 **3.4 From a concentration of 50 µg/mL and below, *C. acnes* EVs do not appear to affect cell**
356 **viability in the two different skin models tested**

357 A cytotoxicity assay was performed in HaCaT and SZ95 immortalized cell lines. In both tests, *C.*
358 *acnes* A1, H1 and H2 EVs were added at different doses (1.56 µg/mL, 3.125 µg/mL, 6.25 µg/mL,
359 12.5 µg/mL, 25 µg/mL, 50 µg/mL, 100 µg/mL and 200 µg/mL). As is shown in Fig. 5A, in the
360 HaCaT model cell viability is not reduced in any condition.
361 On the other hand, in the SZ95 model cell viability is reduced to 50-70% when concentrations of
362 200 µg/mL and 100 µg/mL of EVs are added (Fig. 5B). Nonetheless, in this model when adding
363 concentrations of 50 µg/mL and below, viability is lowered by approximately 15-20% in A1 and
364 H2 EVs but is maintained nearly at 100% in H1 EVs.

365 **3.5 EVs released by *C. acnes* A1, H1 and H2 phylotypes modulate differently the expression**
366 **of biomarkers related to the immune system, oxidative stress, skin barrier and sebum**
367 **production**

368 Different *in vitro* skin models were used to evaluate the immunomodulatory properties of direct
369 stimulation with a range of concentrations of *C. acnes* A1, H1 and H2 EVs (Fig. 1B). In this
370 sense, HaCaT, SZ95 and Jurkat immortalized cell lines were used(Colombo et al., 2017; Hewitt
371 et al., 2013; Kühbacher et al., 2017; Luongo et al., 2014; Nikolakis et al., 2015; Sutterby et al.,
372 2022; Törőcsik et al., 2021). In all *in vitro* models, cells were stimulated with *C. acnes* EVs for
373 24h, and after that, the expression level of different regulatory genes (immune system, skin barrier
374 and oxidative stress) was measured by RT-qPCR. As Fig. 6A shows, A1 EVs trigger a higher
375 stimulation of the pro-inflammatory cytokines Interleukin-8 (IL-8) and TGFβ-1, and the

376 prostaglandin COX-2 which is linked to oxidative stress, compared to H1 or H2 EVs. Regarding
377 genes involved in the reinforcement of the skin barrier, such as occludin, all concentrations of H2
378 EVs and high concentrations of H1 EVs (25 µg/mL and 50 µg/mL) were the only ones able to
379 induce a significant increase in the mRNA expression compared to the negative control. However,
380 for claudin-1, all the conditions seem to activate the expression of this gene, except low doses of
381 H2 EVs, compared to untreated cells. In contrast, expression levels of MMP-2, a matrix
382 metalloproteinase implicated in tissue remodelling (Manuel & Gawronska-Kozak, 2006), did
383 not show marked differences for any of the EVs treatment with respect to the control. Regarding
384 the skin immune system model, as Fig. 6B shows, only A1 EVs triggered a significant expression
385 of the pro-inflammatory cytokine IL-8 compared to the control, while only H1 EVs and high
386 doses of H2 EVs (50 µg/mL) had substantial anti-inflammatory cytokine IL-10 expression.
387 However, for the pro-inflammatory TNFα expression, none of the EVs conditions tested were
388 able to modulate its mRNA levels. As illustrated in Fig. 6C, A1 EVs are constantly triggering
389 greater activation of the inflammatory cytokine IL-8. Otherwise, for the sebum regulator gene
390 PLIN-2 none of the EVs tested were able to substantially stimulate the up-regulation of this gene
391 expression compared to the untreated control.

392 **3.6 EVs derived from *C. acnes* A1 phylotype induce a higher secretion of**
393 **immunomodulatory mediators in three *in vitro* skin models compared to EVs from *C. acnes***
394 **H1 and H2 phylotypes**

395 To confirm the immunomodulatory effects assayed by RT-qPCR in HaCaT, Jurkat and SZ95 *in*
396 *vitro* models, after 24h of incubation with different concentrations of A1, H1 and H2 EVs, the
397 protein secretion levels of some cytokines released in the SN were evaluated by Human High
398 Sensitivity Plex Discovery Assay (Eve Technologies).
399 As shown in Fig. 7A in the HaCaT *in vitro* model, and following the same pattern as for IL-8
400 expression level, A1 EVs displayed the highest secretion of IL-8, IL-6, TNFα and GM-CSF
401 compared to the rest of the EVs, especially when high concentrations of EVs were applied to the

402 keratinocytes. Only 25 and 50 µg/mL for H1 EVs and 50 µg/mL for H2 EVs were able to induce
403 a significant difference in IL-6 secretion compared to the negative control. In the immune system
404 model, composed of Jurkat cells (Fig. 7B), high doses of A1 EVs were observed to trigger
405 increased secretion of IL-8, IL-6 and TNFα compared to the other conditions, but in the case of
406 GM-CSF, H1 and H2 EVs were the ones involved in the activation of this factor. Regarding the
407 SZ95 model (Fig. 7C), IL-8 stimulation correlates with the gene expression data obtained
408 previously. Overall, it can be observed that A1 EVs consistently trigger significant activation of
409 the inflammation-related factors IL-8, IL-6, TNFα and GM-CSF, compared to the negative
410 control. In the case of H1 EVs, only 25 and 50 µg/mL were able to induce significant IL-8 release
411 compared to control.

412 **3.7 *C. acnes* H1 EVs showed to have a better skin sebum inhibition mechanism compared**
413 **to A1 and H2 EVs**

414 The acneic *in vitro* model consisted of a 48-hour treatment with AA5 as a sebum inducer followed
415 by a 24-hour treatment with 12.5 µg/mL of *C. acnes* A1, H1 and H2 EVs. After AA5 incubation,
416 a strong and significant increase in lipid level by about 263-fold was observed, compared to the
417 negative control condition. When PCi-SEB were treated for 24h with 12.5 µg/mL of *C. acnes* A1,
418 H1 and H2 EVs, they showed a 2.8, 4.3 and 3.6-fold reduction *versus* the AA5 condition,
419 respectively. However, although results showed that the three types of EVs had a significant
420 inhibitory effect on sebum production compared to the positive control, the best sebum inhibitory
421 effect was obtained after H1 EVs treatment, with about 4-fold inhibition compared to AA5
422 condition (Fig. 8).

423 **4. DISCUSSION**

424 The Gram-positive bacterium *C. acnes* is one of the main representative genera presents in the
425 human skin microbiota with a key and pivotal role in maintaining a healthy skin barrier. In the
426 same way that occurs in the intestine, communication between C. acnes and host cells it is

427 proposed to be *established* via soluble mediators and EVs that can diffuse through the different
428 layers of the skin (epidermis, dermis and hypodermis). Specifically, EVs act as nano-carriers of
429 proteins, metabolites and nucleic acids upon interaction and internalization into host cells.
430 Therefore, it has been suggested that, considering the cargo of *C. acnes* EVs, they will have a
431 different role, being responsible on the different effects on skin alterations. *C. acnes* strains are
432 currently classified into eight phylotypes (IA1, IA2, IB1, IB2, IB3, IC, II and III), being the IA1
433 and IA2 clades preferentially found in acne lesions whereas phylotype IB is linked to a healthy
434 skin without sign of acne. In this context, where acne vulgaris is the 8th most prevalent disease,
435 with a 9.4% world population affection and without any effective or secure treatment in the
436 market, the objective of this project has been focused on studying the role of EVs secreted by A1
437 (IA1), H1 (IB) and H2 (IB) *C. acnes* phylotypes as a safety biotherapy in cutaneous disorders
438 such acne vulgaris.
439 EV research remains a major challenge due to their intrinsically complex biogenesis, their great
440 heterogeneity in terms of size and the natural variations between batches encountered during their
441 production (Gandham et al., 2020; Hartjes et al., 2019; Paganini et al., 2019). Nevertheless, the
442 nature (small, non-synthetic and non-replicative) of these structures makes them unique to
443 overcome important barriers found in the current dermatology and cosmetic field as it is the skin
444 penetrance, side effects derived from chemicals and maintaining the skin microbiota symbiosis.
445 However, despite this good prognose of EVs used as bio-carriers, what will determine a
446 successful, harmful or poor functionality in terms of acne vulgaris pathology, will depend on the
447 specific cargo of the EVs, which is directly related to the bacterium from which they derive.
448 Therefore, as the main components are proteins, a proteomic characterization of *C. acnes* EVs
449 was performed to determine the relationship of their protein cargo with the skin microbiota. A
450 Venn diagram identified, in agreement with Chudzik et al., 2022, that A1 EVs contain the highest
451 number of proteins, in our case almost four times more proteins than in H1 EVs and nine times
452 more than in H2 EVs. These results were validated with an SDS-PAGE, where the band profile
453 was different between phylotypes (Article). This could be associated with the extra number of
454 pathogenic proteins that EVs of A1 phylotype harbour in contrast to H1 and H2 EVs. In fact,

455 McDowell A. et al, 2013 found that certain strains of *C. acnes* (specifically type IA1) were
456 capable of secreting several virulence factors that enhanced the inflammatory response. However,
457 there are no genetic studies of the *C. acnes* strains used in this work, but as it has been showed
458 previously, H1 has a protective effect against acne vulgaris development, thus we could assume
459 that these two strains could have lost the virulence factors during the evolution. Following this
460 assumption, 25 virulence factors (related to adhesion, biofilm formation, etc.) were found during
461 the mass spectrometry analysis for A1 EVs while only 2 were attributed to H1 and 0 for H2 *C.*
462 *acnes* EVs.
463 Regarding shared proteins by all the *C. acnes* EVs types, the proteomic analysis revealed that a
464 big amount of proteins related to facilitate the transfer of multiple proteins involved in
465 biochemical processes and metabolism between cells, were present in EVs, validating the carrier
466 function of these structures. Moreover, it is known that EVs are used as a way of exchange cell
467 surface substances and improve bacterial survival during infections (Chen et al., 2022), and in
468 this sense we could identified, as described previously by Jeon et al., several proteins used in
469 antibiotic resistance, suggesting that *C.* acnes EVs are also involved in bacterial survival against
470 external threats. In addition, due to the nature and sebum oily niche of *C. acnes*, common proteins
471 involved in lipolysis such as lysophospholipase and triacylglycerol lipase were identified in the
472 EVs. Although these enzymes are generally considered putative virulence factors, lipases are
473 necessary for *C. acnes* to maintain healthy skin by metabolizing sebum and releasing fatty acids,
474 which are necessary to keep a proper skin acidity that acts as a natural barrier against harmful
475 pathogens, providing innate skin immunity (Kim et al., 2020).
476 Considering the analysis of *C. acnes* phylotype-exclusive proteins for A1, H1 and H2 EVs,
477 important differences were found in accordance with previous studies, pointing to *C. acnes*
478 phylogroup A1 (IA1) as an acne-associated group and *C. acnes* phylogroup H1 (IB) as a beneficial
479 and skincare group (Agak et al., 2018; Choi et al., 2018b; Chudzik et al., 2022; Fitz-Gibbon et
480 al., 2013; Liu et al., 2014; Lomholt & Kilian, 2010; McLaughlin et al., 2019; Nakase et al., 2021;
481 O'Neill & Gallo, 2018; Paetzold et al., 2019). As for A1 EVs, its protein profile revealed a great
482 number of proteins involved in bacterial competition and antibiotic resistance (hydrolase,

483 Ppx/GppA phosphatase family, Metallo-ß-lactamase domain protein and histidine kinase)
484 (McLaughlin et al., 2019), biofilm formation (glycosyltransferase and serine/threonine-protein
485 kinase) and virulence (porphyrin, sialidase, HtaA domain protein, phosphoesterase, hydrolase and
486 sigma factor SigA) which were not detected in H1 or H2 EVs. Regarding the exclusive proteins
487 of H1 EVs, different proteins directly involved in fatty acid catabolism were found, such as acyl-
488 CoA dehydrogenase (Swigoňová et al., 2009) and a putative two-component sensor kinase which
489 upregulates the hydrolysis of sebum triglycerides secreting free fatty acids. Indirectly, the N-
490 acetyl-gamma-glutamyl-phosphate reductase, a protein involved in the L-Arginine biosynthetic
491 pathway was also found as part of H1 EVs. In this regard, L-arginine helps to protect the skin
492 from free radicals, increases the skin's visible hydration levels, and potentially supports collagen
493 production (Gad, 2010). All these results indicate that EVs and bacteria from which they derive,
494 share functionalities, and it point to EVs as one of the mechanisms of action by which the specific
495 *C. acnes* strains exert their effect, as it has been previously described by Choi et al., 2018b or
496 Briaud & Carroll, 2020.
497 Then, the next step in our study was to show if the presence of unique peptides in the different
498 types of *C. acnes* EVs could translate, as expected, in different functionalities in the host. For this
499 purpose, an in vitro system representing the pathophysiology derived from acne was used. During
500 acne vulgaris development, as Mattii et al., 2018 showed, not only the external skin layer is
501 affected, having also sebocytes a pivotal role. Nonetheless, unlike most of the publications using
502 skin models are based only in keratinocytes, in this work, other cell types were taken into
503 consideration, as sebocytes and immune cells, to have a closer picture of what is happening in
504 real skin during acne vulgaris. To do that, different in vitro assays were carried out. Regarding
505 cytotoxicity assays, they revealed that doses of 50 µg/mL and below of *C. acnes* EVs did not
506 appear to affect cell viability either in the HaCaT model or in the SZ95 model, thus deeming them
507 as safe to be tested in the in vitro skin models. Comparing both cell types, it was also observed
508 that sebocytes were more responsive than keratinocytes. This can be explained because sebocytes
509 inhabit in the sebaceous gland, which is located in the dermis, protected from external microbes
510 in contrast to keratinocytes exposed and in constantly interaction with skin microorganisms.

511 Then, the different EVs were directly incubated for 24h in the different in vitro models: a) the
512 outer layer skin model consisted of HaCaT cells to mimic the epidermis composed mainly of
513 keratinocytes; b) the sebum model consisted of SZ95 cells to mimic the sebaceous gland
514 environment and c) the broken barrier skin model, consisting of Jurkat cells, was chosen to get an
515 idea of when the skin barrier is disrupted, one of the severe attributes of inflammatory skin
516 diseases. The expression levels of different regulatory genes were measured by RT-qPCR and
517 results displayed that, as previously was showed by Nagy et al., 2005, in all in vitro skin models,
518 A1 EVs were systematically triggering increased activation of pro-inflammatory cytokines (Nagy
519 et al., 2005). This could be due to the presence of a large number of virulence factors found in the
520 proteomic analysis for A1 EVs. On the other side, in the broken skin barrier model, H1 EVs and
521 50 µg/mL doses of H2 EVs induced a significant expression of the anti-inflammatory cytokine
522 IL-10, reinforcing the possible protective role of these two non-pathogenic strains during acne
523 vulgaris development.
524 To cross-check the immunomodulatory effects assayed by gene expression, the protein secretion
525 levels of some cytokines released in the SN of the *in vitro* models were evaluated and it was
526 confirmed that EVs derived from *C. acnes* A1 induce a higher secretion of immunomodulatory
527 mediators in the three *in vitro* skin models compared to *C. acnes* H1 and H2 EVs. According to
528 the RT-qPCR results, it was determined that A1 EVs consistently triggered a higher activation of
529 the inflammation-related factors IL-8, IL-6, TNFα and GM-CSF, compared to H1 and H2.
530 The pathophysiology of acne includes, apart from local inflammation, a hyperproduction of
531 sebum by sebocytes which causes specific strains of *C. acnes* to overgrow causing a dysbiosis
532 and triggering the development of acne (Paetzold et al., 2019; Rozas et al., 2021). In fact, one of
533 the most prescribed treatments for dermatologists against acne is based on isotretionin, a retinoid
534 which causes the apoptosis of skin sebocytes to reduce the amount of sebum (Zouboulis, 2006).
535 However, the regulation of sebum during acne development modulated by the skin microbiota is
536 a very new topic and there are few publications on the subject. Therefore, an acneic-mimicking
537 skin model with PCi-SEB and AA5 as sebum inductor, was used to explore the effect of *C. acnes*
538 EVs on sebum regulation. After 24-hour treatment with 12.5 µg/mL of *C. acnes* A1, H1 and H2

539 EVs, results showed that the three types of EVs had a significant inhibitory effect on sebum
540 production compared to the positive control, highlighting that the best inhibition was obtained
541 after H1 EVs treatment, with inhibition by about 4 folds compared to the positive control. These
542 results were expected and in accordance with the proteomic analysis that described H1 EVs as
543 being charged with exclusive proteins with lipidomic effect.
544 To our knowledge, this is the first study in which proteomic characterization of three different
545 phylotypes of *C. acnes* has been performed, in addition to the testing of three different *C. acnes*
546 phylotypes in different *in vitro* skin models. This work has proved that *C. acnes* EVs are more
547 than lipid spheres that act as mechanisms of action of the derived bacteria. Specially H1 EVs has
548 been highlighted as the best bioactive nanocarrier, counteracting acne symptomatology from two
549 flanks, inhibiting inflammation and modulating sebum production.
550

551 **5. CONCLUSION**

552 The findings of this project have shown that *C. acnes* EVs are key intermediators in the
553 communication between skin microbiota and the host, having an essential role during skin
554 alterations such as acne vulgaris. In this sense, these results point to H1 EVs as a potential,
555 efficient, safe and based-natural treatment to prevent and ameliorate symptomatology associated
556 with inflammation and oily skin. However, further scientific experiments need to be done
557 including assays with primary cell lines, *in vivo* animal models, checking EVs stability in a gel
558 cream and performing clinical tests to extend the knowledge and to have the whole picture of how
559 *C. acnes* EVs act on the skin.
560

561 **ABBREVIATIONS**

562 *C. acnes: Cutibacterium acnes*
563 EVs: extracellular vesicles
564 PBS: phosphate-buffered saline
565 SN: supernatant

566 TEM: transmission electron microscopy

567 NTA: nanoparticle tracking analysis

568 SDS-PAGE: sodium dodecyl sulfate-polyacrylamide gel electrophoresis

569 PBS: phosphate-buffered saline

570 CPS: cycles per second

571 DDA: data-dependent acquisition

572 AGC: auto gain control

573 HCD: high-energy collision dissociation

574 FDR: false discovery rate

575 XIC: extracted ion current

576 ATCC: American Type Culture Collection

577 DMEM: Dulbecco's Modified Eagle Medium

578 FBS: Fetal Bovine Serum

579 EGFr: recombinant human epidermal growth factor

580 $CaCl_2$: calcium chloride

581 RPMI: Roswell Park Memorial Institute medium

582 RT: room temperature

583 WGA: wheat germ agglutinin

584 RT-qPCR: quantitative real time-PCR analysis

585 PCi-SEB: human iPSC-derived sebocytes

586 AA5: 5 μM of arachidonic acid

587 SD: standard deviation

588 GO: Gene Ontology

589 IL: interleukin

590 CITE: biofilm matrix dynamics

591 **ETHICS APPROVAL AND CONSENT TO PARTICIPATE**

592 Not applicable

CONSENT FOR PUBLICATION

All authors give their consent for publication of this work in Microbiome as a research article.

AVAILABILITY OF DATA AND MATERIALS

The raw data from proteomic analysis are included as Supporting Tables S1, S2 and S3.

The original R scripts for plotting the extracellular vesicle data are available on Bitbucket. (https://bitbucket.org/synbiolab/fabrega_vesicles/src/master/)

COMPETING INTERESTS

The authors declare that they have not competing interests

FUNDING INFORMATION

This work was funded and supported by the University Pompeu Fabra – Excelencia Maria de Maeztu Post-doctoral program (CEX 2018-0007392-M). NK is funded by a Maria Maetzu-UPF fellowship (Catalan Government) and by the Sociedad Española de Químicos Cosméticos (SEQC) and MJF is funded by a Juan de la Cierva Fellowship from the Spanish Government (Award FJC 2018-037096-I).

AUTHOR'S CONTRIBUTIONS

M.P. participated in the experimental laboratory work, data curation, formal analysis, writing the main manuscript text and preparing all figures. J.M. did the bioinformatic analysis, prepared figure 3 and helped with the writing of the original draft. L.T. and N.K. participated in the experimental laboratory work, specially helping to set up the in vitro assays and bacterial cultures. J.M. participated in the experimental laboratory work, developing the in vitro acneic model and preparing figure 8. M.G. contributed supervising the project and helping to write the main manuscript text. M.F. helped with the experimental laboratory work, data curation, formal

615 analysis, writing the manuscript, doing the funding acquisition/project administration, and
616 supervising the project.

617 **ACKNOWLEDGEMENT**

618 We want to express our deepest gratitude to Dr. Bernhard Paetzold for generously providing *C.*
619 *acnes* strains used in this study and also Dr. Jordi García-Ojalvo for mentoring this project. We
620 also want to thanks the Office Naval Research (Award N62909-18-1-2155) for giving us the
621 opportunity to study how to work with anaerobic skin bacteria.

622 **CONFLICT OF INTEREST**

623 The authors report no conflict of interest.

624
625 **REFERENCES**
626

627 Agak, G. W., Kao, S., Ouyang, K., Qin, M., Moon, D., Butt, A., & Kim, J. (2018). Phenotype and
628 Antimicrobial Activity of Th17 Cells Induced by Propionibacterium acnes Strains
629 Associated with Healthy and Acne Skin. *Journal of Investigative Dermatology*, *138*(2),
630 316–324. https://doi.org/10.1016/j.jid.2017.07.842
631 Bajic, S. S., Cañas, M. A., Tolinacki, M., Badia, J., Sánchez, B., Golic, N., Margolles, A.,
632 Baldomá, L., & Ruas-Madiedo, P. (2020). Proteomic profile of extracellular vesicles
633 released by Lactiplantibacillus plantarum BGAN8 and their internalization by non-polarized
634 HT29 cell line. *Scientific Reports*, *10*(1). https://doi.org/10.1038/s41598-020-78920-z
635 Blum, H. E. (2017). The human microbiome. In *Advances in Medical Sciences* (Vol. 62, Issue 2,
636 pp. 414–420). Medical University of Bialystok.
637 https://doi.org/10.1016/j.advms.2017.04.005
638 Briaud, P., & Carroll, R. K. (2020). Extracellular vesicle biogenesis and functions in gram-
639 positive bacteria. *Infection and Immunity*, *88*(12). https://doi.org/10.1128/IAI.00433-
640 20/FORMAT/EPUB
641 Brown, L., Wolf, J. M., Prados-Rosales, R., & Casadevall, A. (2015). Through the wall:
642 Extracellular vesicles in Gram-positive bacteria, mycobacteria and fungi. In *Nature Reviews*
643 *Microbiology* (Vol. 13, Issue 10, pp. 620–630). Nature Publishing Group.
644 https://doi.org/10.1038/nrmicro3480
645 Cañas, M. A., Giménez, R., Fábrega, M. J., Toloza, L., Baldomà, L., & Badia, J. (2016). Outer
646 membrane vesicles from the probiotic Escherichia coli Nissle 1917 and the commensal
647 ECOR12 enter intestinal epithelial cells via clathrin-dependent endocytosis and elicit
648 differential effects on DNA damage. *PLoS ONE*, *11*(8).
649 https://doi.org/10.1371/journal.pone.0160374

Chen, J., Zhang, H., Wang, S., Du, Y., Wei, B., Wu, Q., & Wang, H. (2022). Inhibitors of Bacterial Extracellular Vesicles. *Frontiers in Microbiology*, *13*. https://doi.org/10.3389/fmicb.2022.835058

Choi, E. J., Lee, H. G., Bae, I. H., Kim, W., Park, J., Lee, T. R., & Cho, E. G. (2018a). Propionibacterium acnes-Derived Extracellular Vesicles Promote Acne-Like Phenotypes in Human Epidermis. *Journal of Investigative Dermatology*, *138*(6), 1371–1379. https://doi.org/10.1016/j.jid.2018.01.007

Choi, E. J., Lee, H. G., Bae, I. H., Kim, W., Park, J., Lee, T. R., & Cho, E. G. (2018b). Propionibacterium acnes-Derived Extracellular Vesicles Promote Acne-Like Phenotypes in Human Epidermis. *Journal of Investigative Dermatology*, *138*(6), 1371–1379. https://doi.org/10.1016/J.JID.2018.01.007

Christensen, G. J. M., Scholz, C. F. P., Enghild, J., Rohde, H., Kilian, M., Thürmer, A., Brzuszkiewicz, E., Lomholt, H. B., & Brüggemann, H. (2016). Antagonism between Staphylococcus epidermidis and Propionibacterium acnes and its genomic basis. *BMC Genomics*, *17*(1). https://doi.org/10.1186/s12864-016-2489-5

Chudzik, A., Migdał, P., & Paściak, M. (2022). Different Cutibacterium acnes Phylotypes Release Distinct Extracellular Vesicles. *International Journal of Molecular Sciences*, *23*(10), 5797. https://doi.org/10.3390/ijms23105797

Colombo, I., Sangiovanni, E., Maggio, R., Mattozzi, C., Zava, S., Corbett, Y., Fumagalli, M., Carlino, C., Corsetto, P. A., Scaccabarozzi, D., Calvieri, S., Gismondi, A., Taramelli, D., & Dell'Agli, M. (2017). HaCaT Cells as a Reliable in Vitro Differentiation Model to Dissect the Inflammatory/Repair Response of Human Keratinocytes. *Mediators of Inflammation*, *2017*. https://doi.org/10.1155/2017/7435621

Eisenstein, M. (2020). The skin microbiome. *Nature Outlines*, *588*, S209.

Fábrega, M. J., Rodríguez-Nogales, A., Garrido-Mesa, J., Algieri, F., Badía, J., Giménez, R., Gálvez, J., & Baldomà, L. (2017). Intestinal anti-inflammatory effects of outer membrane vesicles from Escherichia coli Nissle 1917 in DSS-experimental colitis in mice. *Frontiers in Microbiology*, *8*(JUL). https://doi.org/10.3389/fmicb.2017.01274

Fitz-Gibbon, S., Tomida, S., Chiu, B. H., Nguyen, L., Du, C., Liu, M., Elashoff, D., Erfe, M. C., Loncaric, A., Kim, J., Modlin, R. L., Miller, J. F., Sodergren, E., Craft, N., Weinstock, G. M., & Li, H. (2013). Propionibacterium acnes strain populations in the human skin microbiome associated with acne. *Journal of Investigative Dermatology*, *133*(9), 2152–2160. https://doi.org/10.1038/jid.2013.21

Gad, M. Z. (2010). Anti-aging effects of L-arginine. In *Journal of Advanced Research* (Vol. 1, Issue 3, pp. 169–177). https://doi.org/10.1016/j.jare.2010.05.001

Gandham, S., Su, X., Wood, J., Nocera, A. L., Alli, S. C., Milane, L., Zimmerman, A., Amiji, M., & Ivanov, A. R. (2020). Technologies and Standardization in Research on Extracellular Vesicles. In *Trends in Biotechnology* (Vol. 38, Issue 10, pp. 1066–1098). Elsevier Ltd. https://doi.org/10.1016/j.tibtech.2020.05.012

Hartjes, T. A., Mytnyk, S., Jenster, G. W., van Steijn, V., & van Royen, M. E. (2019). Extracellular vesicle quantification and characterization: Common methods and emerging approaches. In *Bioengineering* (Vol. 6, Issue 1). MDPI AG. https://doi.org/10.3390/bioengineering6010007

Hewitt, N. J., Edwards, R. J., Fritsche, E., Goebel, C., Aeby, P., Scheel, J., Reisinger, K., Ouédraogo, G., Duche, D., Eilstein, J., Latil, A., Kenny, J., Moore, C., Kuehnl, J., Barroso, J., Fautz, R., & Pfuhler, S. (2013). Use of human in Vitro skin models for accurate and ethical risk assessment: Metabolic considerations. *Toxicological Sciences*, *133*(2), 209–217. https://doi.org/10.1093/toxsci/kft080

Kim, S. Y., Kim, M. H., Son, J. H., Kim, S. il, Yun, S. H., Kim, K., Kim, S., Shin, M., & Lee, J. C. (2020). Outer membrane vesicles produced by Burkholderia cepacia cultured with subinhibitory concentrations of ceftazidime enhance pro-inflammatory responses. *Virulence*, *11*(1), 995–1005. https://doi.org/10.1080/21505594.2020.1802193

Kühbacher, A., Sohn, K., Burger-Kentischer, A., & Rupp, S. (2017). Immune cell-supplemented human skin model for studying fungal infections. In *Methods in Molecular Biology* (Vol. 1508, pp. 439–449). Humana Press Inc. https://doi.org/10.1007/978-1-4939-6515-1_25

Liu, J., Cheng, A., Bangayan, N. J., Barnard, E., Curd, E., Craft, N., & Li, H. (2014). Draft genome sequences of Propionibacterium acnes type strain ATCC6919 and antibiotic-resistant strain HL411PA1. *Genome Announcements*, *2*(4). https://doi.org/10.1128/genomeA.00740-14

Lomholt, H. B., & Kilian, M. (2010). Population genetic analysis of Propionibacterium acnes identifies a subpopulation and epidemic clones associated with acne. *PLoS ONE*, *5*(8). https://doi.org/10.1371/journal.pone.0012277

Luongo, D., Russo, R., Balestrieri, A., Marzocco, S., Bergamo, P., & Severino, L. (2014). In vitro study of AFB1 and AFM1 effects on human lymphoblastoid Jurkat T-cell model. *Journal of Immunotoxicology*, *11*(4), 353–358. https://doi.org/10.3109/1547691X.2013.848250

Manuel, J. A., & Gawronska-Kozak, B. (2006). Matrix metalloproteinase 9 (MMP-9) is upregulated during scarless wound healing in athymic nude mice. *Matrix Biology*, *25*(8), 505–514. https://doi.org/10.1016/j.matbio.2006.07.008

Mattii, M., Lovászi, M., Garzorz, N., Atenhan, A., Quaranta, M., Lauffer, F., Konstantinow, A., Küpper, M., Zouboulis, C. C., Kemeny, L., Eyerich, K., Schmidt-Weber, C. B., Törőcsik, D., & Eyerich, S. (2018). Sebocytes contribute to skin inflammation by promoting the differentiation of T helper 17 cells. *British Journal of Dermatology*, *178*(3), 722–730. https://doi.org/10.1111/bjd.15879

McDowell, A., Nagy, I., Magyari, M., Barnard, E., & Patrick, S. (2013). The Opportunistic Pathogen Propionibacterium acnes: Insights into Typing, Human Disease, Clonal Diversification and CAMP Factor Evolution. *PLoS ONE*, *8*(9). https://doi.org/10.1371/journal.pone.0070897

McLaughlin, J., Watterson, S., Layton, A. M., Bjourson, A. J., Barnard, E., & McDowell, A. (2019). Propionibacterium acnes and acne vulgaris: New insights from the integration of population genetic, multi-omic, biochemical and host-microbe studies. In *Microorganisms* (Vol. 7, Issue 5). MDPI AG. https://doi.org/10.3390/microorganisms7050128

Nagy, I., Pivarcsi, A., Koreck, A., Széll, M., Urbán, E., & Kemény, L. (2005). Distinct strains of Propionibacterium acnes induce selective human β-defensin-2 and interleukin-8 expression in human keratinocytes through toll-like receptors. *Journal of Investigative Dermatology*, *124*(5), 931–938. https://doi.org/10.1111/j.0022-202X.2005.23705.x

Nakase, K., Koizumi, J., Midorikawa, R., Yamasaki, K., Tsutsui, M., Aoki, S., Nasu, Y., Hirai, Y., Nakaminami, H., & Noguchi, N. (2021). Cutibacterium acnes phylogenetic type IC and II isolated from patients with non-acne diseases exhibit high-level biofilm formation. *International Journal of Medical Microbiology*, *311*(7). https://doi.org/10.1016/j.ijmm.2021.151538

Nikolakis, G., Seltmann, H., Hossini, A. M., Makrantonaki, E., Knolle, J., & Zouboulis, C. C. (2015). Ex vivo human skin and SZ95 sebocytes exhibit a homoeostatic interaction in a novel coculture contact model. *Experimental Dermatology*, *24*(7), 497–502. https://doi.org/10.1111/exd.12712

O'Neill, A. M., & Gallo, R. L. (2018). Host-microbiome interactions and recent progress into understanding the biology of acne vulgaris. In *Microbiome* (Vol. 6, Issue 1). BioMed Central Ltd. https://doi.org/10.1186/s40168-018-0558-5

Paetzold, B., Willis, J. R., Pereira De Lima, J., Knödlseder, N., Brüggemann, H., Quist, S. R., Gabaldón, T., & Güell, M. (2019). Skin microbiome modulation induced by probiotic solutions. *Microbiome*, *7*(1). https://doi.org/10.1186/s40168-019-0709-3

Paganini, C., Capasso Palmiero, U., Pocsfalvi, G., Touzet, N., Bongiovanni, A., & Arosio, P. (2019). Scalable Production and Isolation of Extracellular Vesicles: Available Sources and Lessons from Current Industrial Bioprocesses. In *Biotechnology Journal* (Vol. 14, Issue 10). Wiley-VCH Verlag. https://doi.org/10.1002/biot.201800528

Rackaityte, E., & Lynch, S. v. (2020). The human microbiome in the 21st century. In *Nature Communications* (Vol. 11, Issue 1). Nature Research. https://doi.org/10.1038/s41467-020-18983-8

Rozas, M., de Ruijter, A. H., Fabrega, M. J., Zorgani, A., Guell, M., Paetzold, B., & Brillet, F. (2021). From dysbiosis to healthy skin: Major contributions of cutibacterium acnes to skin homeostasis. In *Microorganisms* (Vol. 9, Issue 3, pp. 1–18). MDPI AG. https://doi.org/10.3390/microorganisms9030628

Shu, M., Wang, Y., Yu, J., Kuo, S., Coda, A., Jiang, Y., Gallo, R. L., & Huang, C. M. (2013). Fermentation of Propionibacterium acnes, a Commensal Bacterium in the Human Skin Microbiome, as Skin Probiotics against Methicillin-Resistant Staphylococcus aureus. *PLoS ONE*, *8*(2). https://doi.org/10.1371/journal.pone.0055380

Sutterby, E., Thurgood, P., Baratchi, S., Khoshmanesh, K., & Pirogova, E. (2022). Evaluation of in vitro human skin models for studying effects of external stressors and stimuli and developing treatment modalities. *VIEW*, *3*(2), 20210012. https://doi.org/10.1002/viw.20210012

Swigoňová, Z., Mohsen, A. W., & Vockley, J. (2009). Acyl-coA dehydrogenases: Dynamic history of protein family evolution. *Journal of Molecular Evolution*, *69*(2), 176–193. https://doi.org/10.1007/s00239-009-9263-0

Törőcsik, D., Fazekas, F., Póliska, S., Gregus, A., Janka, E. A., Dull, K., Szegedi, A., Zouboulis, C. C., & Kovács, D. (2021). Epidermal Growth Factor Modulates Palmitic Acid-Induced Inflammatory and Lipid Signaling Pathways in SZ95 Sebocytes. *Frontiers in Immunology*, *12*. https://doi.org/10.3389/fimmu.2021.600017

Zouboulis, C. C. (2006). Isotretinoin revisited: Pluripotent effects on human sebaceous gland cells. In *Journal of Investigative Dermatology* (Vol. 126, Issue 10, pp. 2154–2156). Nature Publishing Group. https://doi.org/10.1038/sj.jid.5700418

FIGURES AND FIGURE LEGENDS

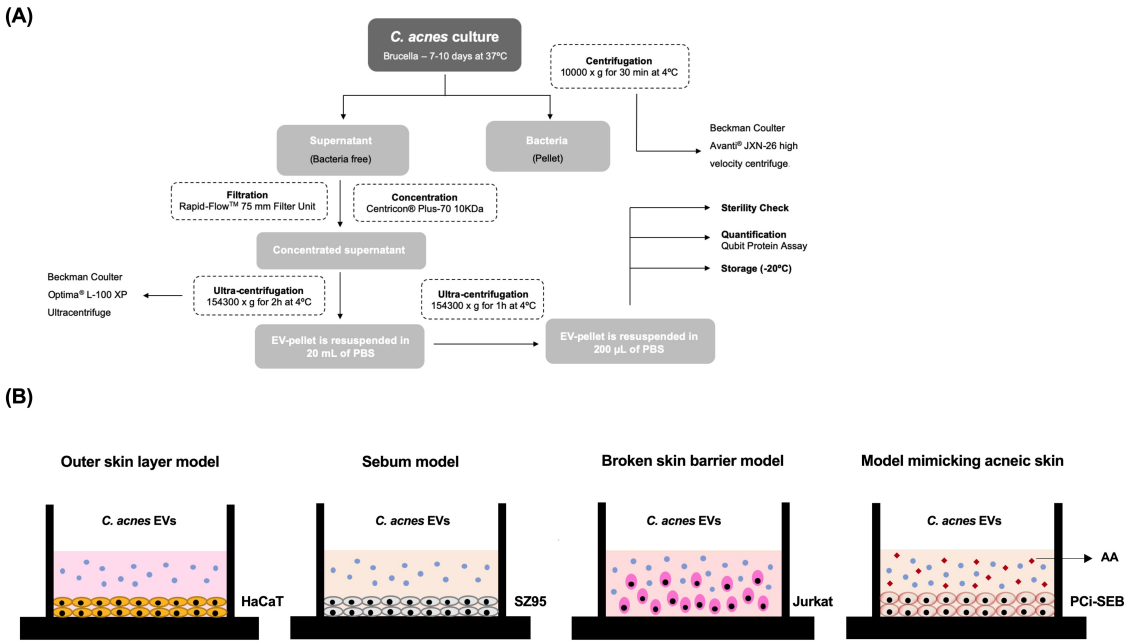

Fig. 1. **EVs isolation protocol and *in vitro* experimental design**. (A) Process to isolate C. acnes-derived extracellular vesicles (EVs). (B) Schematic presentation of the different skin in vitro models: the outer skin layer model with HaCaT cell line, the sebum model with SZ95 cell line, the broken skin barrier model with Jurkat cells and the acneic skin model with PCi-SEB cells using AA to induce sebum production.

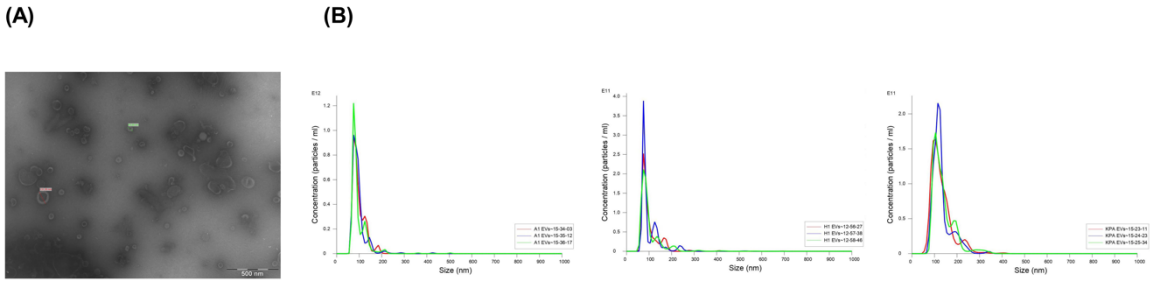

Fig. 2. Visualization of *C. acnes* EVs by different microscopy techniques. (A) Transmission Electron Microscopy of C. acnes H1 EVs (bar 500 nm). (B) Nanoparticle Tracking Analysis of *C. acnes* A1, H1 and H2 EVs. Prior to the measurement, the samples were diluted in PBS buffer at 1:5000, 1:1000 and 1:1000 respectively. EVs have a mean diameter of 96.8 ± 0.5 nm, 100.7 ± 0.7 nm and 133.0 ± 2.3 nm respectively. EV-concentration is expressed as a number of particles per mL on the y axis. All data represent the mean of three independent experiments ± standard error.

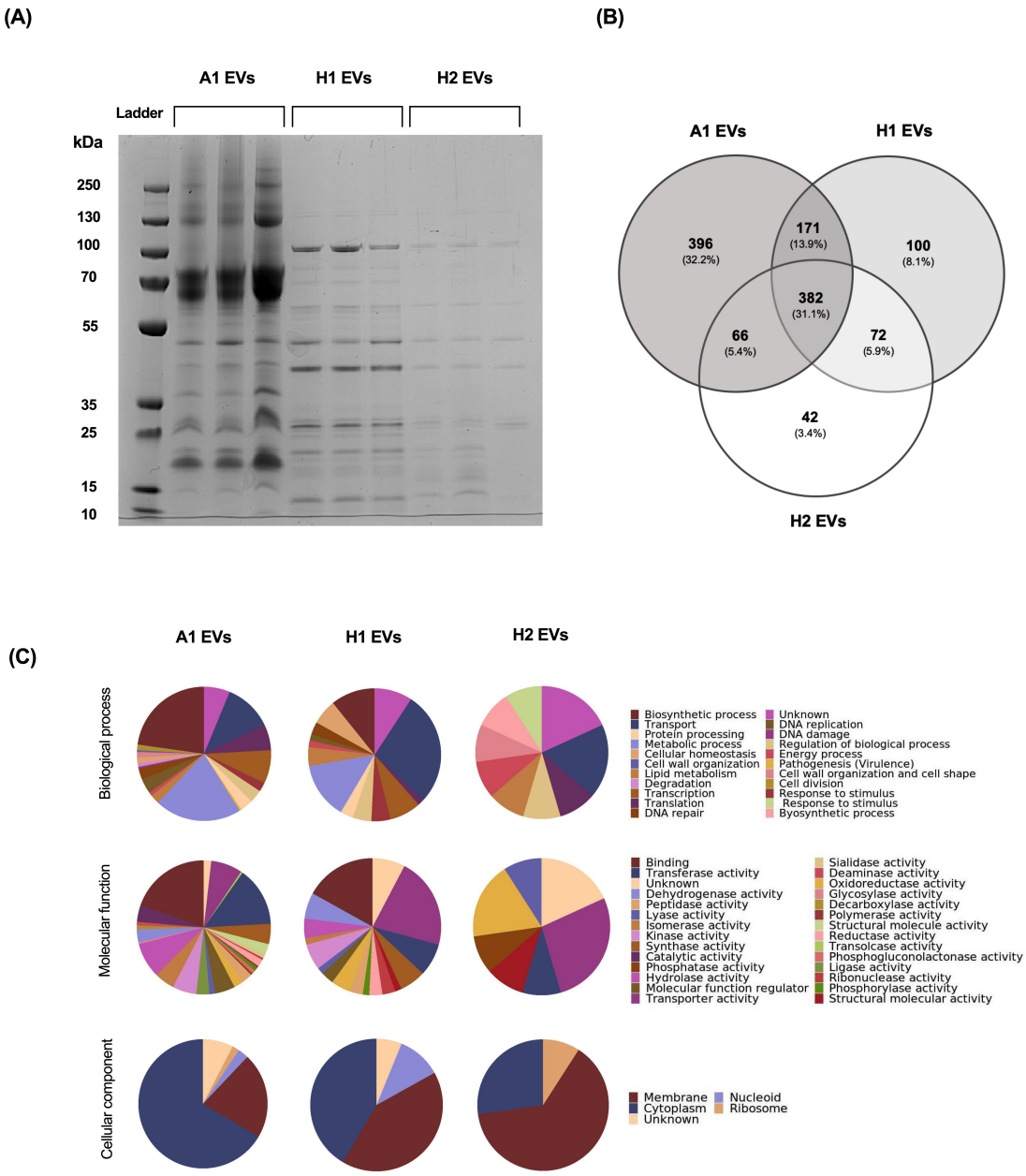

Fig. 3. Proteomic characterization of *C. acnes* A1, H1 and H2 EVs. (A) Proteomic fingerprint of *C. acnes* EVs. SDS-PAGE gel showing protein bands of triplicates from EVs of different phylotypes. A concentration of 7 µg of total amount of protein was loaded in a NuPage 4 to 12% Bis-Tris gel and stained with Coomassie Brilliant Blue R-250 staining solution. (B) Venn diagram of the proteins contained in *C. acnes* A1, H1 and H2 EVs. The number of overlapping proteins between the different phylotypes is indicated. All data is obtained from three independent experiments. (C) Gene Ontology analysis of *C. acnes* A1, H1 and H2 EVs preparations. Biological process, Molecular function and Cellular components of the identified vesicular proteins in *C. acnes* EVs are presented here. For each *C. acnes* phylotype, three independent batches were analysed in the proteomic analysis.

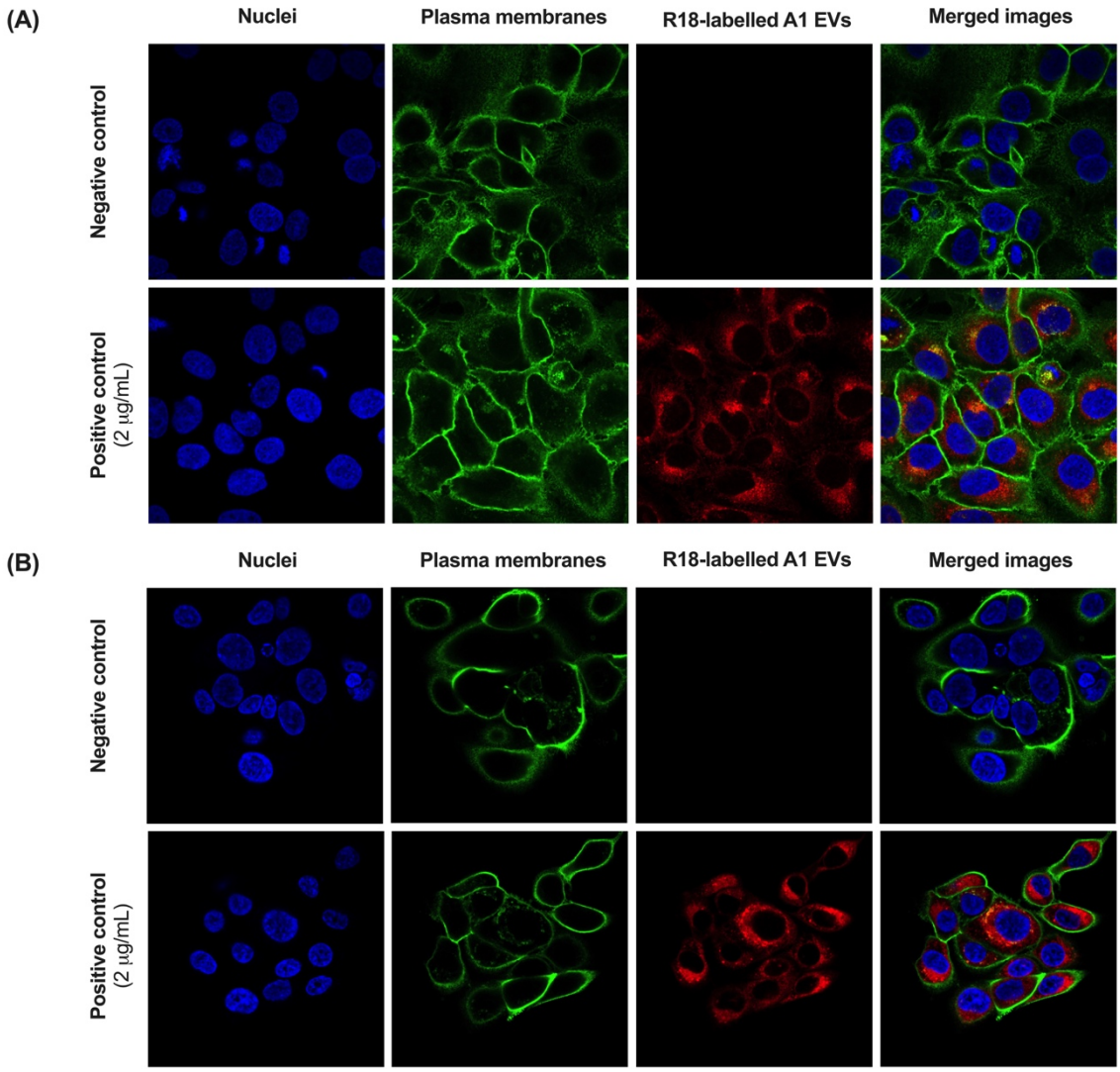

Fig. 4. Uptake of *C. acnes* A1 EVs in (A) HaCaT cell line and (B) SZ95 cell line. Visualization of internalized EVs by confocal fluorescence microscopy. Both cell lines were incubated for 24h at 37°C with rhodamine B-R18-labelled A1 EVs (2 µg/ well).

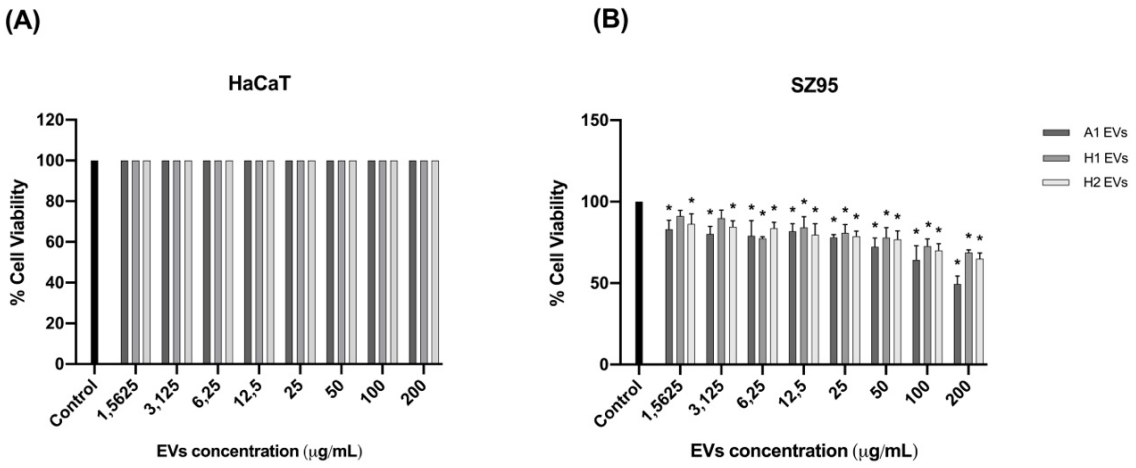

Fig. 5. Cytotoxicity assay of (A) HaCaT cell line and (B) SZ95 cell line treated with different doses of *C. acnes* A1, H1 and H2 EVs. All data are presented as mean ± standard deviation (SD) of triplicate measurements (*$p \leq 0.05$ versus non-stimulated controls).

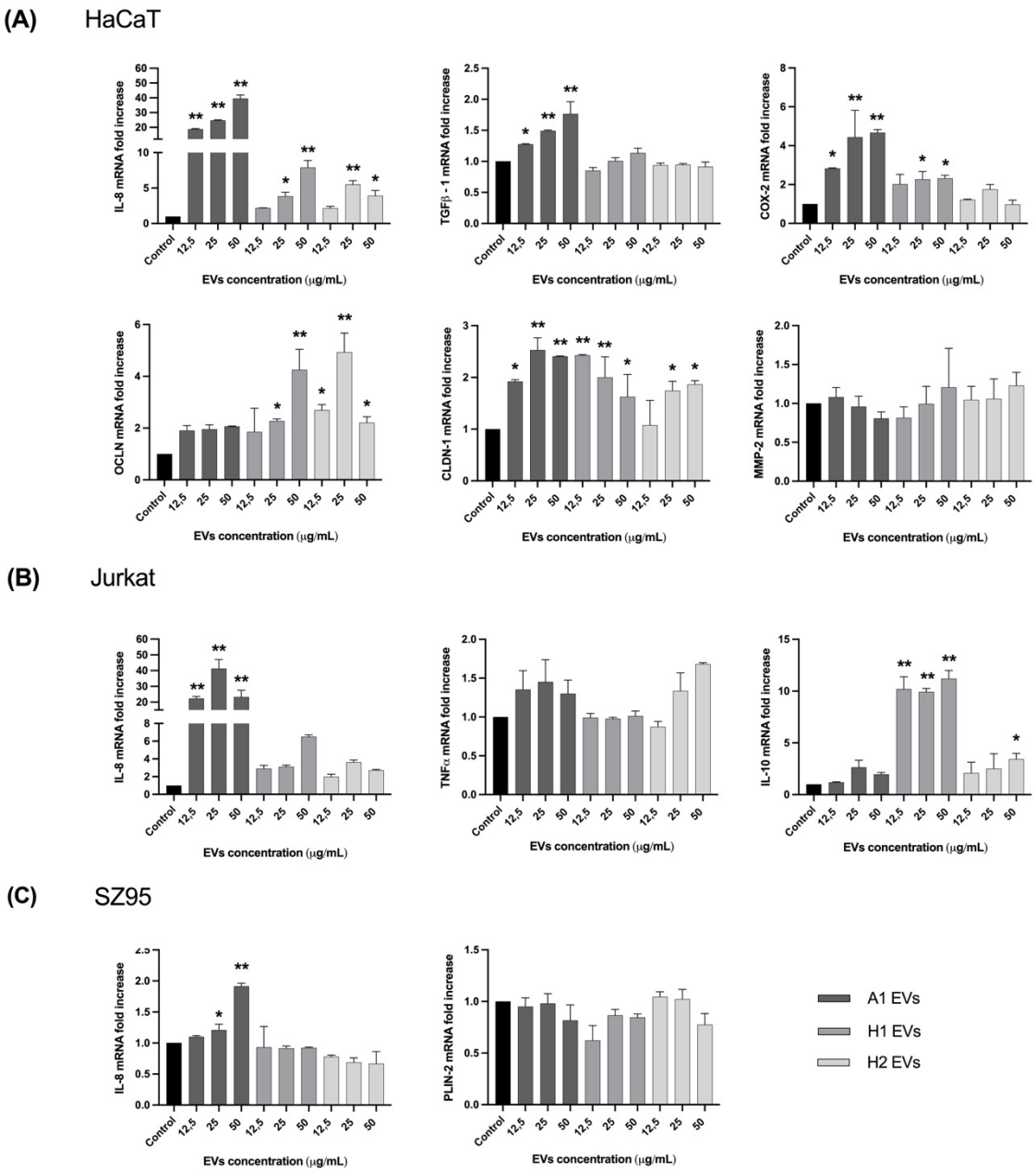

Fig. 6. ***In vitro*** **analysis with direct incubation of** ***C. acnes*** **EVs.** Human cells were treated for 24h with different concentrations (12.5, 25 and 50 µg/mL) of *C. acnes* A1, H1 and H2 EVs. Total RNA was extracted and different biomarkers were assessed by RT-qPCR. (A) HaCaT (B) SZ95 and (C) Jurkat immortalized cell lines. All data are presented as mean ± standard deviation (SD) of triplicate measurements (*$p \leq 0.05$, **$p \leq 0.001$ versus non-stimulated controls).

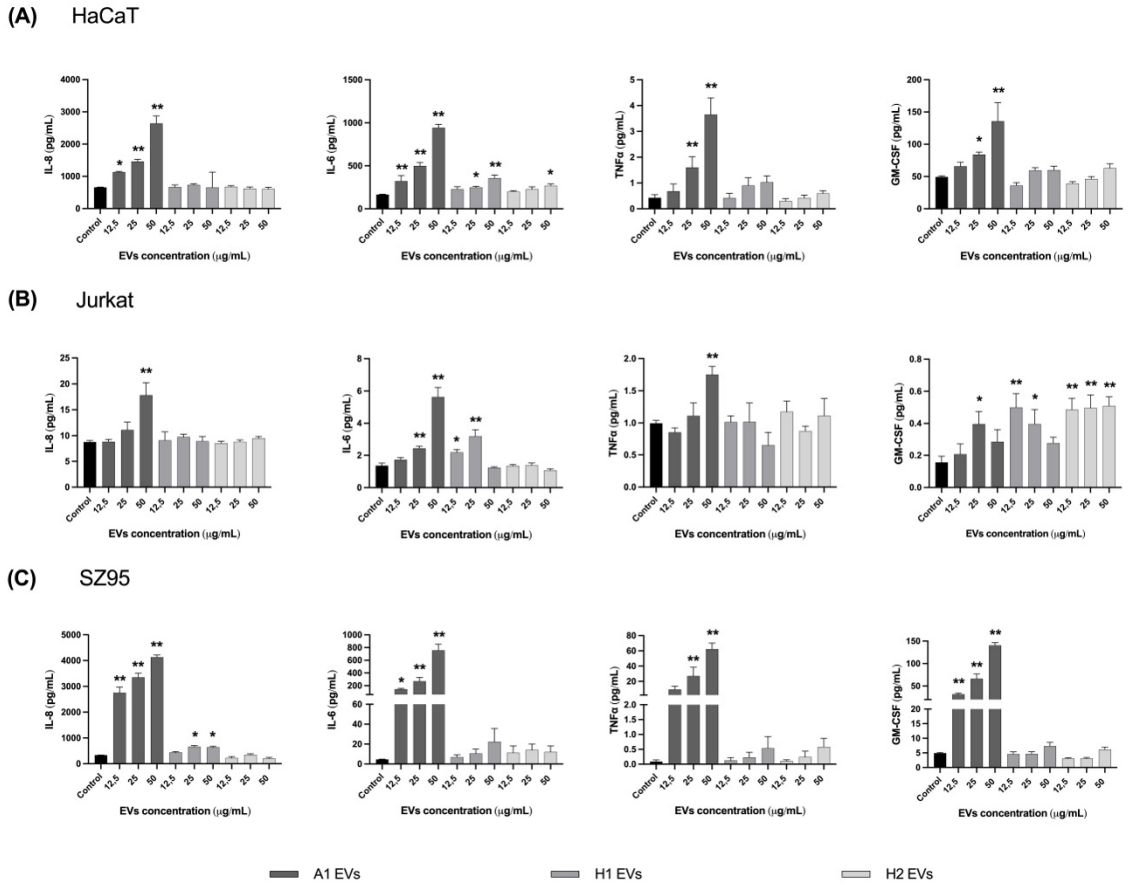

Fig. 7. Total protein concentration secreted into the SN after direct incubation with *C. acnes* EVs. Human cells were treated for 24h with different concentrations (12.5, 25 and 50 µg/mL of *C. acnes* A1, H1 and H2 EVs. Filtered SN was evaluated by Multiplex analysis to measure protein secreted in it. Ranges for the standard curve for each of the biomarkers were: GM-CSF: 0.31 - 4978.62 pg/mL, TNF alpha: 0.11 - 1699.58 pg/mL and IL-6: 0.05 - 768.83 pg/mL. (A) HaCaT (B) SZ95 and (C) Jurkat immortalized cell lines were used. All data are presented as mean ± standard deviation (SD) of triplicate measurements (*$p \leq 0.05$, **$p \leq 0.001$ versus non-stimulated controls).

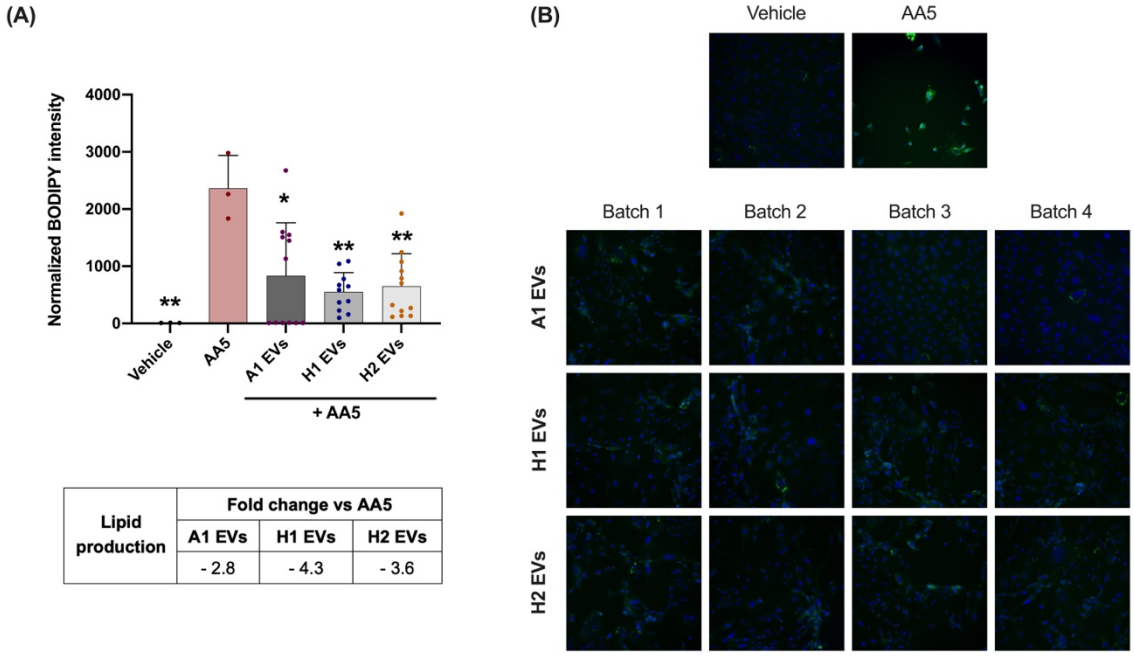

Lipid production	Fold change vs AA5		
	A1 EVs	H1 EVs	H2 EVs
	- 2.8	- 4.3	- 3.6

Fig. 8. Reduction of lipid production was assessed after treating PCi-SEB with AA5 for 24h. PCi-SEB were treated during 48h with AA at 5 µM (AA5) to induce lipid production. Afterwards PCi-SEB were treated for 24h with 12.5 µg/mL of *C. acnes* A1, H1 and H2 EVs (A) Metadata analysis inter-EVs batches and (B) Fluorescence microscopy image of PCi-SEB stained with BODIPY 493/503; negative control (Vehicle), positive control (AA5). All data are presented as mean ± standard deviation (SD) of triplicate measurements (*$p \leq 0.05$, **$p \leq 0.001$ versus non-stimulated controls).

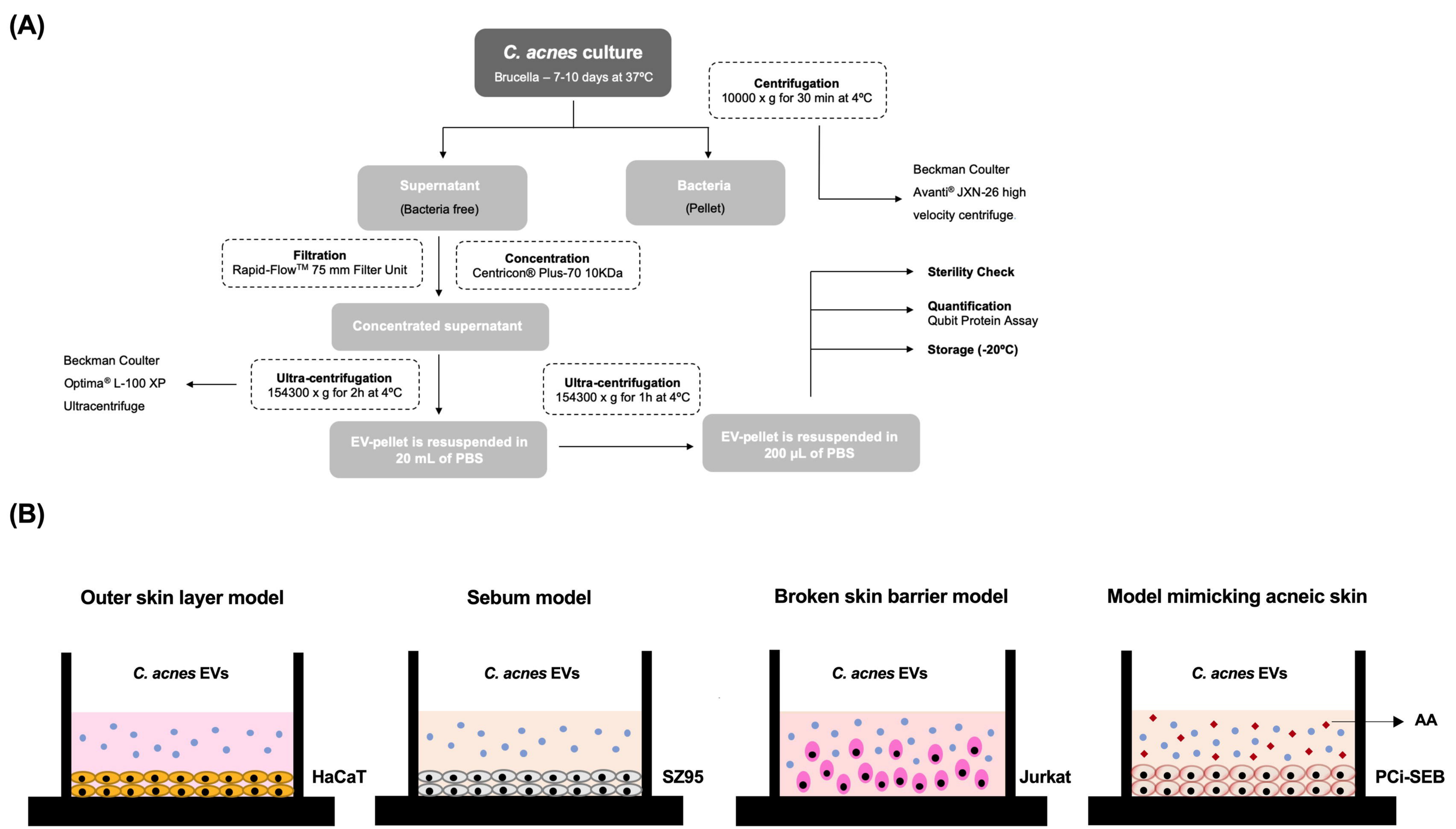
(A)
C. acnes culture
Brucella – 7-10 days at 37ºC
Centrifugation
10000 x g for 30 min at 4ºC
Supernatant
(Bacteria free)
Bacteria
(Pellet)
Beckman Coulter
Avanti® JXN-26 high
velocity centrifuge.
Filtration
Rapid-Flow™ 75 mm Filter Unit
Concentration
Centricon® Plus-70 10KDa
Sterility Check
Quantification
Qubit Protein Assay
Storage (-20ºC)
Concentrated supernatant
Beckman Coulter
Optima® L-100 XP
Ultracentrifuge
Ultra-centrifugation
154300 x g for 2h at 4ºC
Ultra-centrifugation
154300 x g for 1h at 4ºC
EV-pellet is resuspended in
20 mL of PBS
EV-pellet is resuspended in
200 µL of PBS
(B)
Outer skin layer model
Sebum model
Broken skin barrier model
Model mimicking acneic skin
C. acnes EVs
HaCaT
C. acnes EVs
SZ95
C. acnes EVs
Jurkat
C. acnes EVs
AA
PCi-SEB

(A)

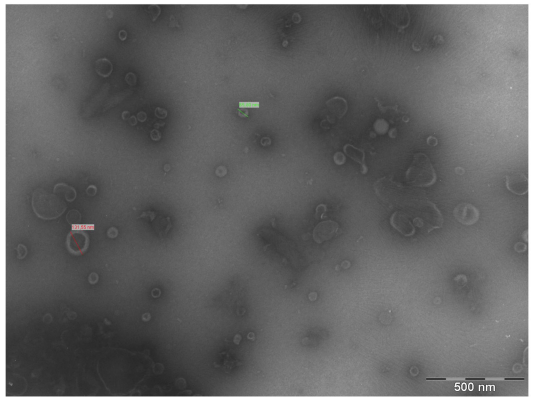
500 nm

(B)

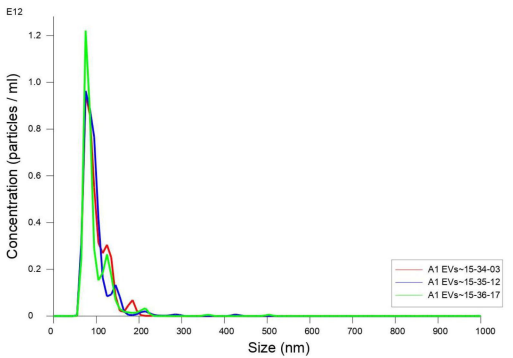
E12
Concentration (particles / ml)
Size (nm)
A1 EVs~15-34-03
A1 EVs~15-35-12
A1 EVs~15-36-17

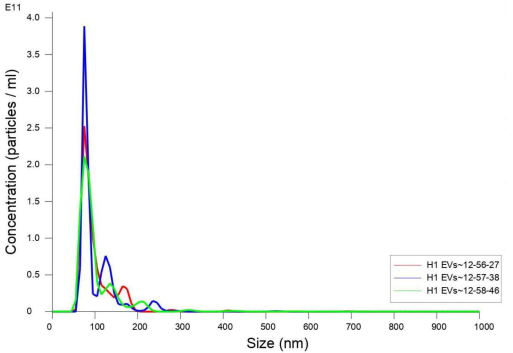
E11
Concentration (particles / ml)
Size (nm)
H1 EVs~12-56-27
H1 EVs~12-57-38
H1 EVs~12-58-46

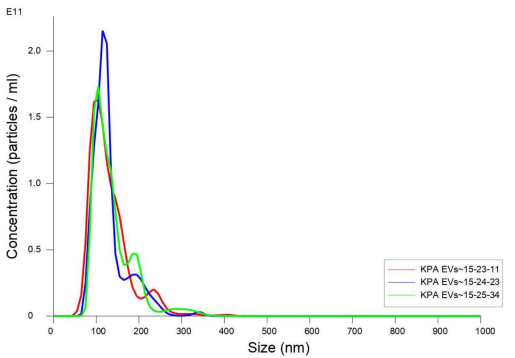
E11
Concentration (particles / ml)
Size (nm)
KPA EVs~15-23-11
KPA EVs~15-24-23
KPA EVs~15-25-34

(A)

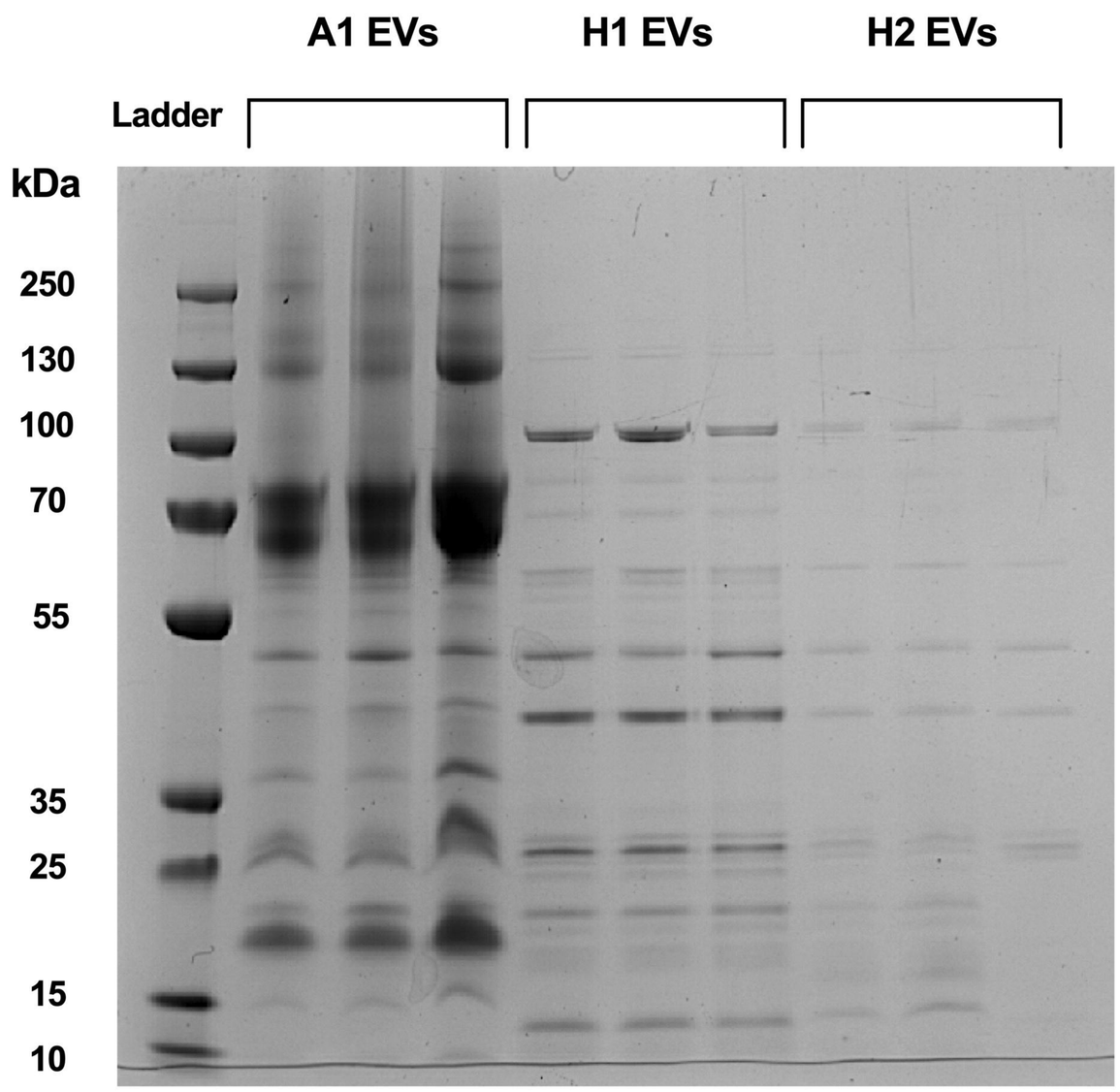
A1 EVs
H1 EVs
H2 EVs
Ladder
kDa
250
130
100
70
55
35
25
15
10

(B)

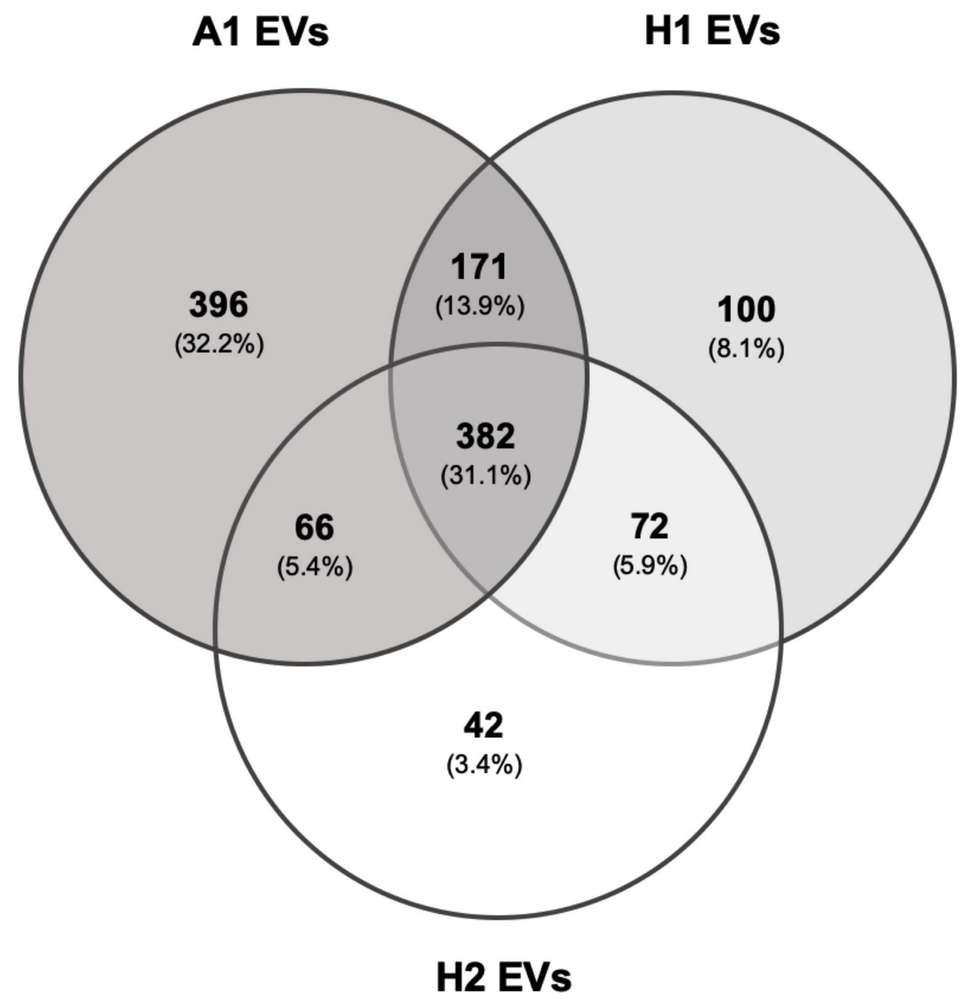
A1 EVs
H1 EVs
H2 EVs
396
(32.2%)
171
(13.9%)
100
(8.1%)
382
(31.1%)
66
(5.4%)
72
(5.9%)
42
(3.4%)

(C)

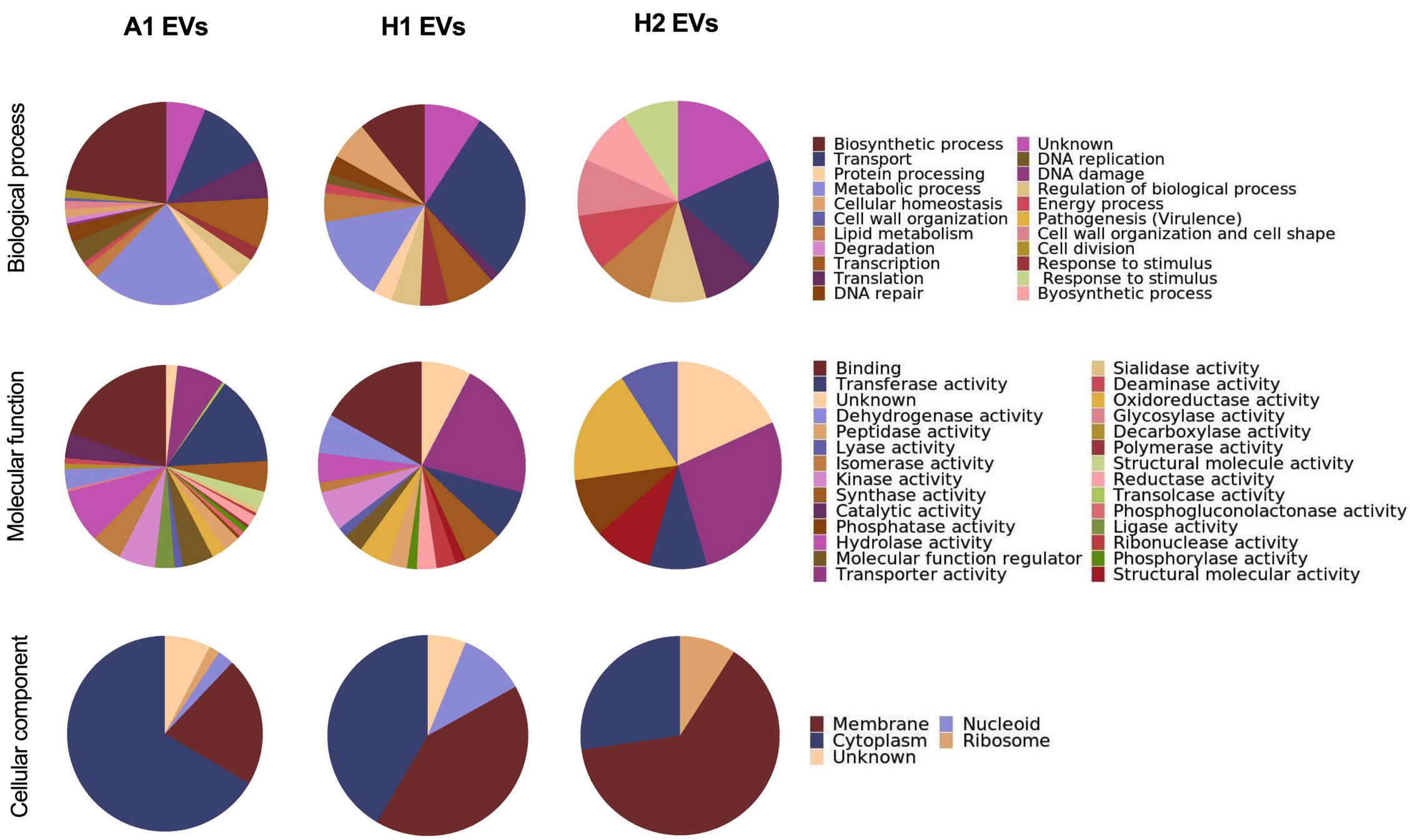
A1 EVs
H1 EVs
H2 EVs
Biological process
Molecular function
Cellular component
Biosynthetic process
Transport
Protein processing
Metabolic process
Cellular homeostasis
Cell wall organization
Lipid metabolism
Degradation
Transcription
Translation
DNA repair
Unknown
DNA replication
DNA damage
Regulation of biological process
Energy process
Pathogenesis (Virulence)
Cell wall organization and cell shape
Cell division
Response to stimulus
Response to stimulus
Byosynthetic process
Binding
Transferase activity
Unknown
Dehydrogenase activity
Peptidase activity
Lyase activity
Isomerase activity
Kinase activity
Synthase activity
Catalytic activity
Phosphatase activity
Hydrolase activity
Molecular function regulator
Transporter activity
Sialidase activity
Deaminase activity
Oxidoreductase activity
Glycosylase activity
Decarboxylase activity
Polymerase activity
Structural molecule activity
Reductase activity
Transolcase activity
Phosphogluconolactonase activity
Ligase activity
Ribonuclease activity
Phosphorylase activity
Structural molecular activity
Membrane
Cytoplasm
Unknown
Nucleoid
Ribosome

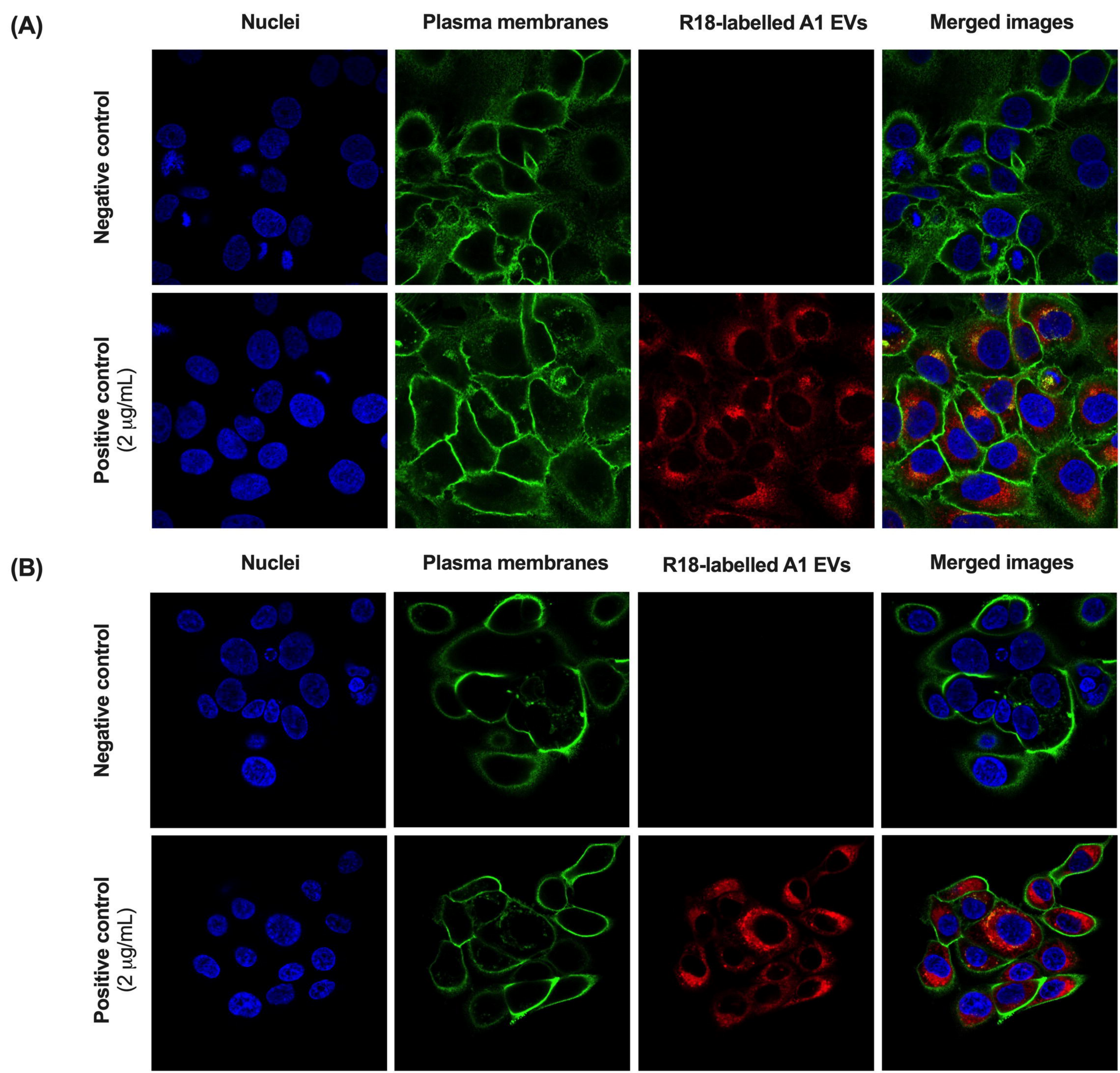
(A)
Nuclei
Plasma membranes
R18-labelled A1 EVs
Merged images
Negative control
Positive control
(2 μg/mL)
(B)
Nuclei
Plasma membranes
R18-labelled A1 EVs
Merged images
Negative control
Positive control
(2 μg/mL)

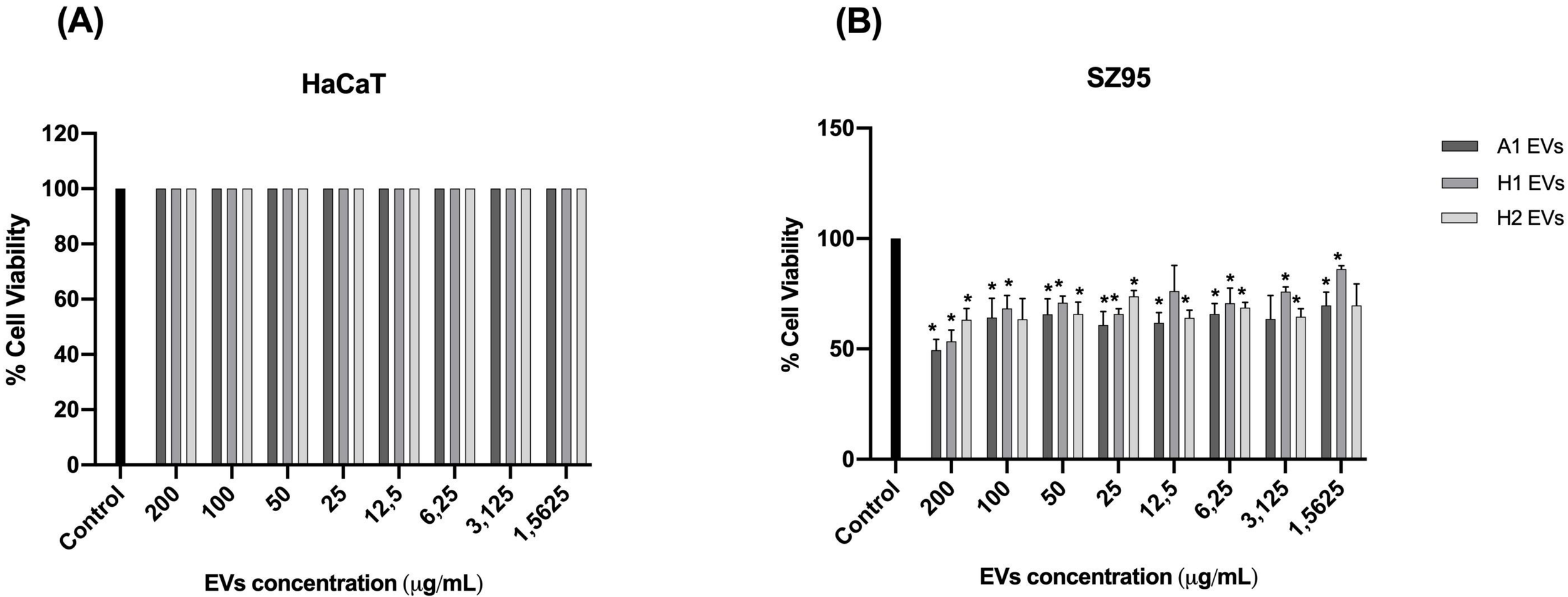
(A)
HaCaT
% Cell Viability
120
100
80
60
40
20
0
Control
200
100
50
25
12,5
6,25
3,125
1,5625
EVs concentration (μg/mL)
(B)
SZ95
% Cell Viability
150
100
50
0
Control
200
100
50
25
12,5
6,25
3,125
1,5625
EVs concentration (μg/mL)
A1 EVs
H1 EVs
H2 EVs

(A) HaCaT

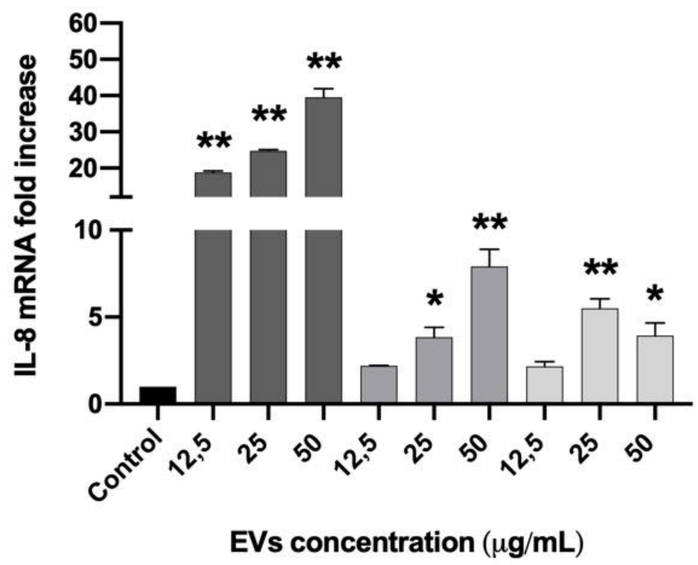

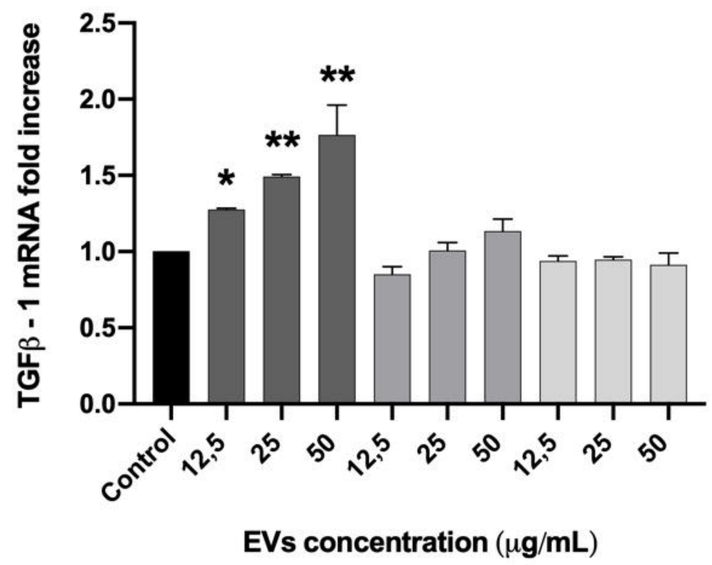

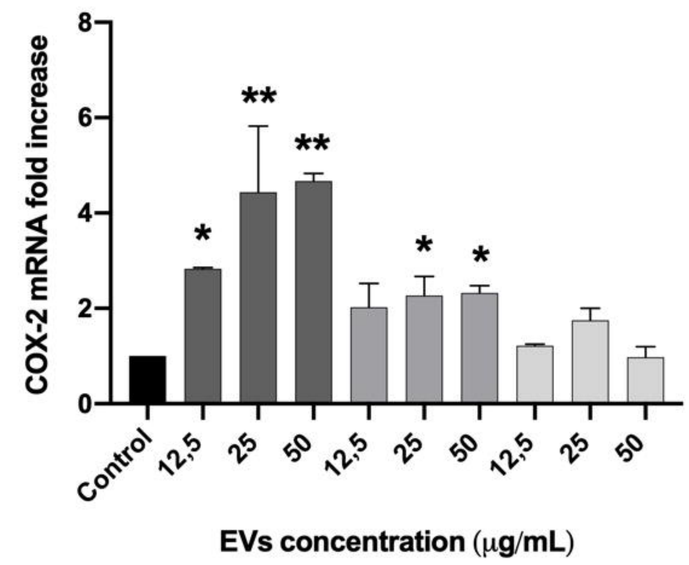

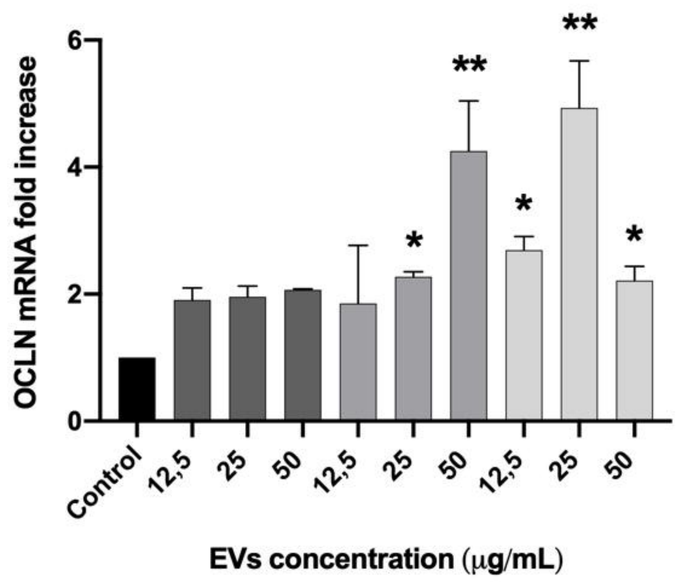

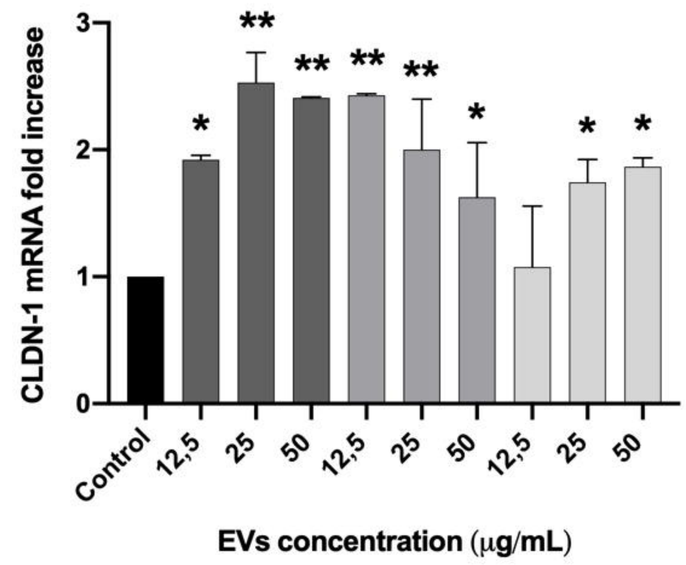

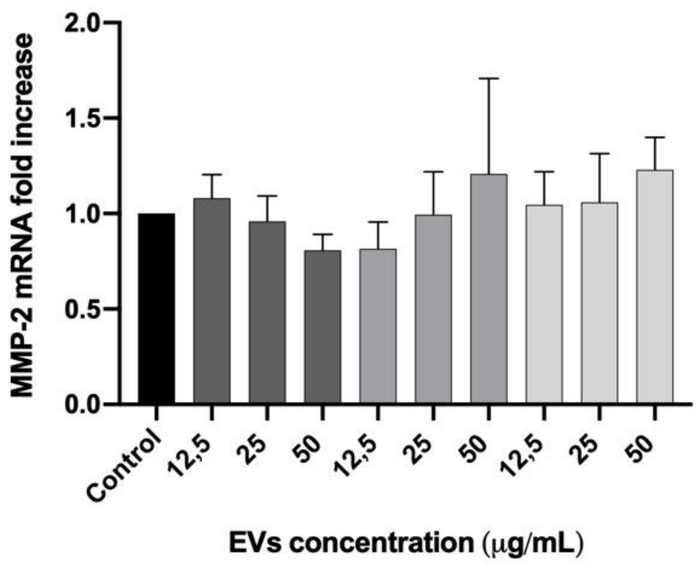

(B) Jurkat

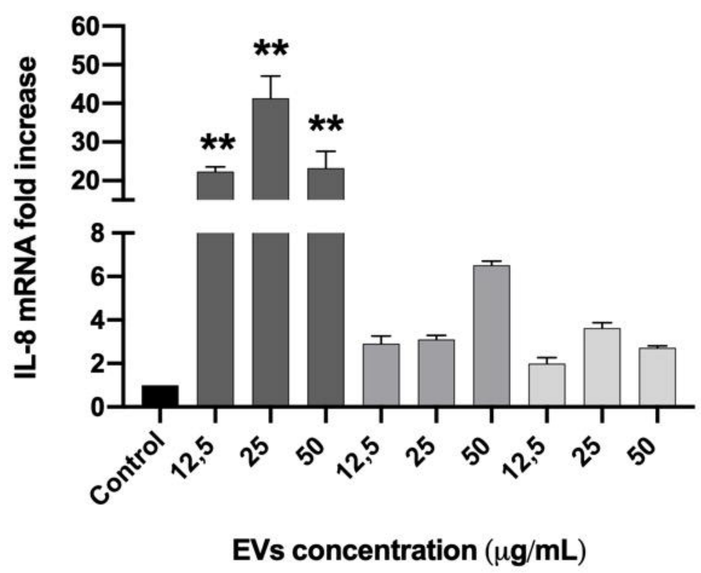

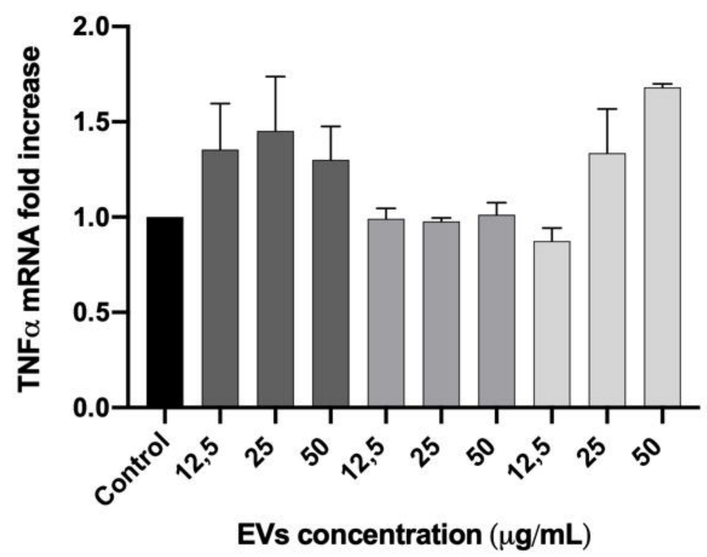

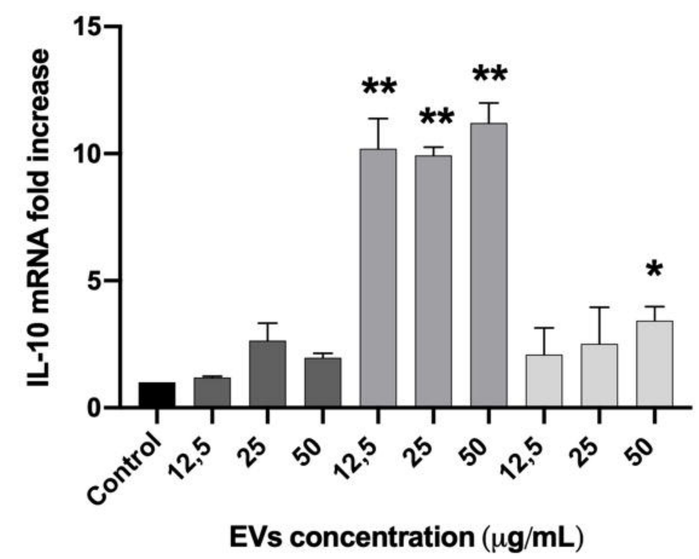

(C) SZ95

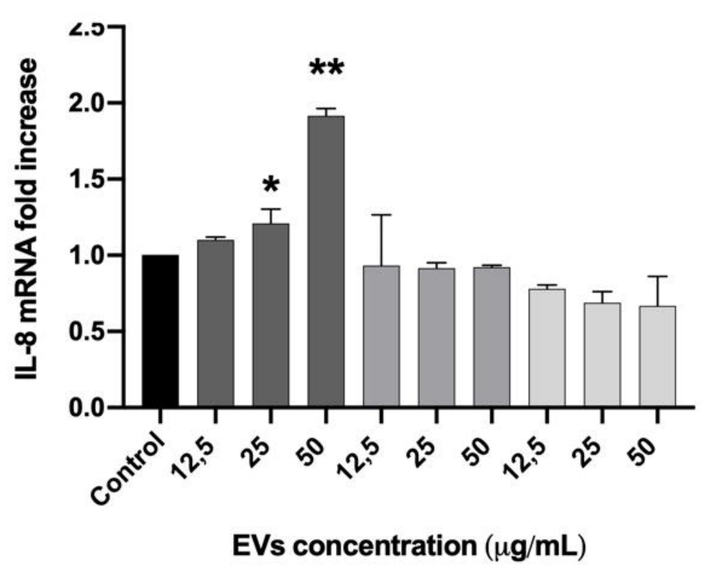

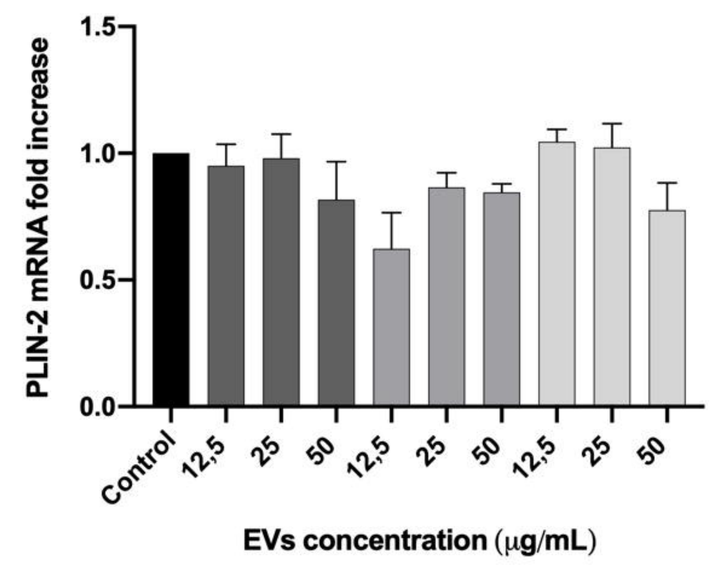

A1 EVs
H1 EVs
H2 EVs

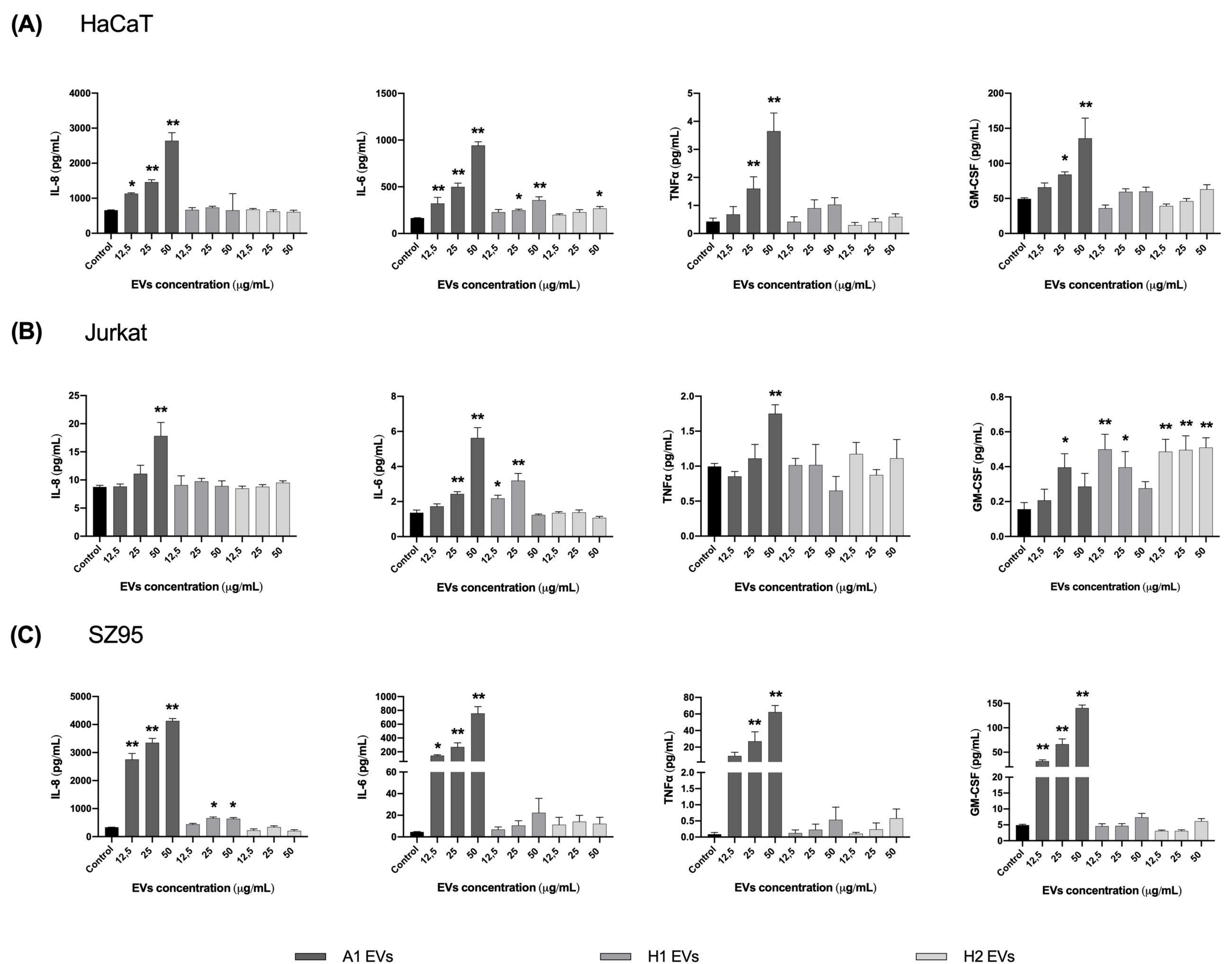
(A) HaCaT
IL-8 (pg/mL)
IL-6 (pg/mL)
TNFα (pg/mL)
GM-CSF (pg/mL)
EVs concentration (μg/mL)
Control
12,5
25
50
(B) Jurkat
(C) SZ95
A1 EVs
H1 EVs
H2 EVs

(A)

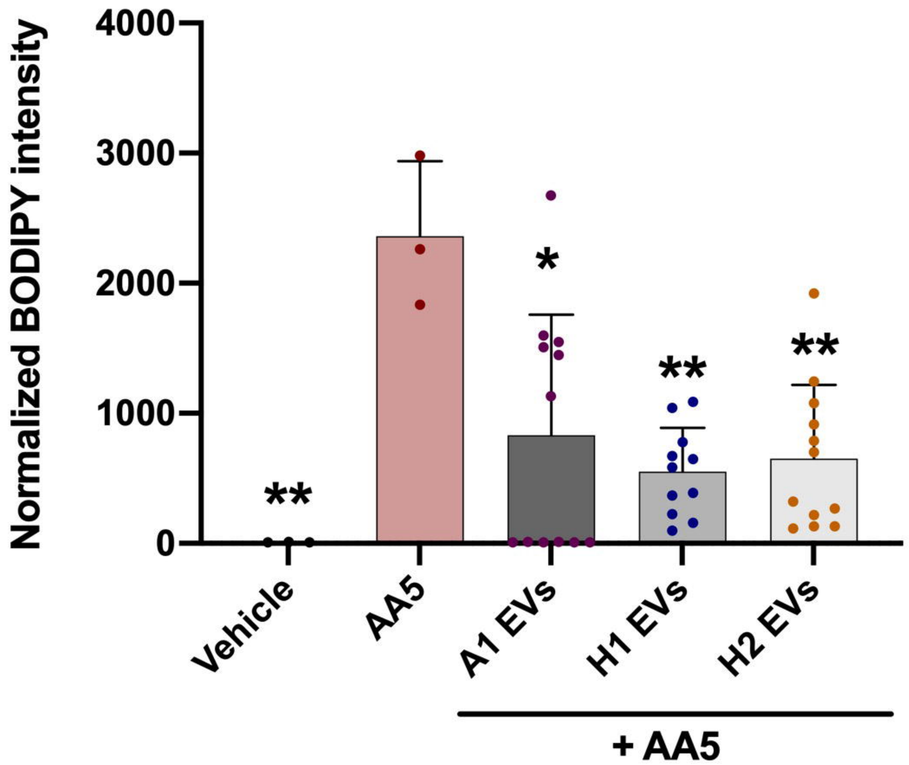

Lipid production	Fold change vs AA5		
	A1 EVs	H1 EVs	H2 EVs
	- 2.8	- 4.3	- 3.6
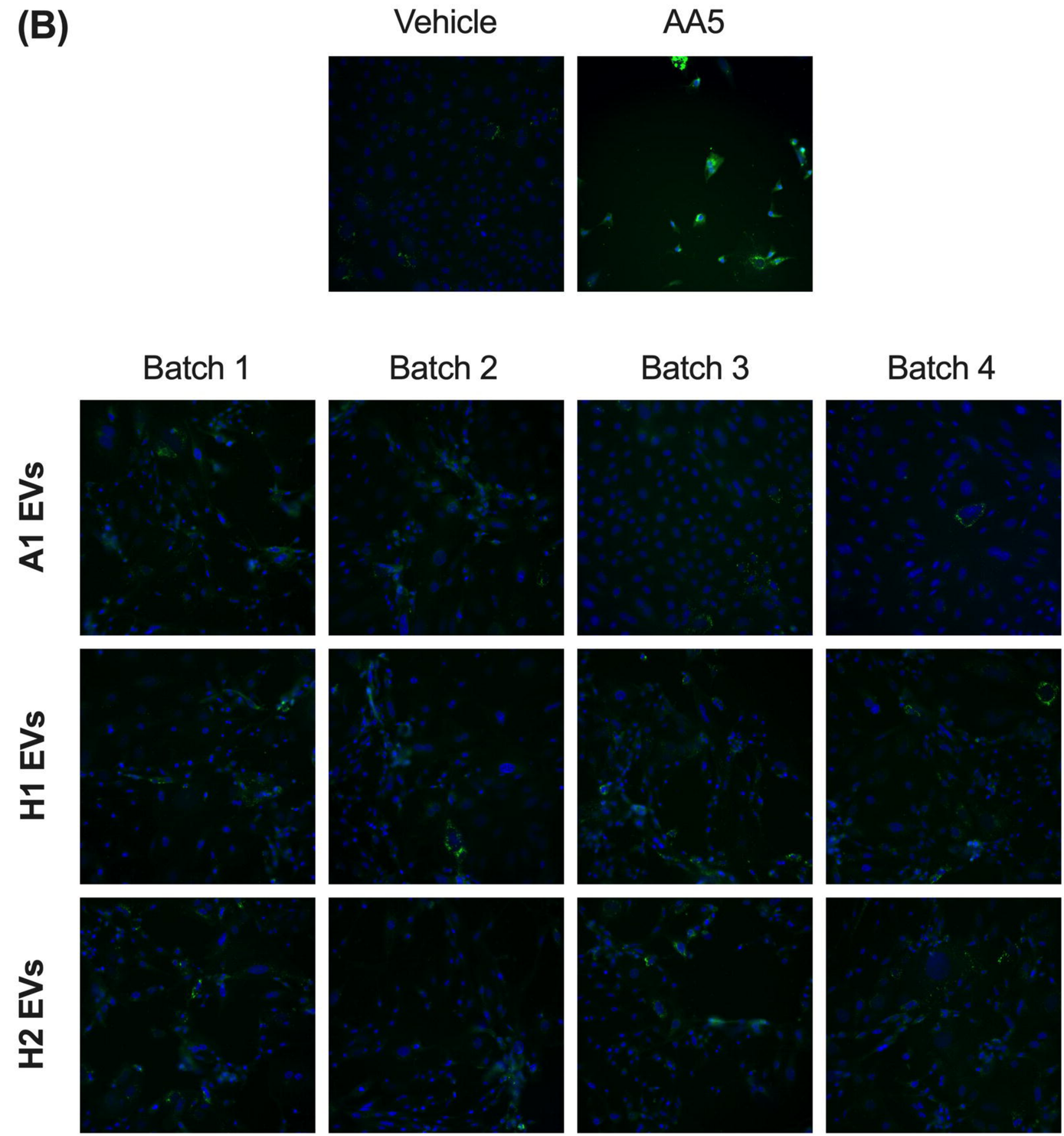
(B)